Applied Catalysis B: Environmental 325 (2023) 122335

Contents lists available at ScienceDirect

Applied Catalysis B: Environmental

journal homepage: www.elsevier.com/locate/apcatb

Highly active hydrogen generation from sodium borohydride methanolysis and ethylene glycolysis reactions using protonated chitosan-zeolite hybrid metal-free particles

Cafer SAKA

Faculty of Health Sciences, Siirt University, 56100 Siirt, Turkey

ARTICLE INFO

Keywords:
Metal-free catalysts
Chitosan-zeolite
Protonation
$NaBH_4$ methanolysis
$NaBH_4$ ethylene glycolysis
Hydrogen

ABSTRACT

Herein, the synthesis of low-cost, non-toxic and recyclable protonated chitosan-zeolite hybrid metal-free catalysts was carried out. The metal-free hybrid catalysts were used for the first time for efficient H_2 production from $NaBH_4$ methanolysis and ethylene glycolysis. The prepared chitosan-zeolite-H composite was characterized by X-ray powder diffraction (XRD), scanning electron microscopy (SEM), energy dispersive X-Ray analyser (EDS), Fourier-transform infrared spectroscopy (FTIR), Transmission electron microscopy (TEM), Brunauer-Emmett-Teller (BET) and X-ray photoelectron spectroscopy (XPS) analyses. The different chitosan/zeolite ratios and different calcination temperatures, the effect of temperature and $NaBH_4$ amount and reusability parameters were investigated. Also, the possible mechanism of H_2 formation in methanol and ethylene glycol with chitosan-zeolite-H is discussed. HGR values of $NaBH_4$ (0.25 g) methanolysis and ethylene glycolysis were 17,500 and 10,428 ml $min^{-1}g^{-1}$, respectively. Ea values obtained for the $NaBH_4$ methanolysis and ethylene glycolysis were found to be 37.29 kJ mol^{-1} and 50.00 kJ mol^{-1}, respectively.

1. Introduction

Interest in alternative clean energy sources continues to increase today and this interest will continue to increase in the future. Hydrogen energy, which has advantages such as high efficiency and non-toxicity, comes to the fore among alternative energy types. However, this H_2 production has its problems such as transportation and storage systems. $NaBH_4$ compound, which is among the chemical hydrides commonly preferred in H_2 production, has preferred properties such as chemical stability, H_2 density up to 10.8% w/w, reasonable price and non-toxic by-products [1,2]. H_2 production from $NaBH_4$ hydrolysis has been widely preferred by researchers [3–7]. However, H_2 production from $NaBH_4$ hydrolysis has disadvantages such as slow reaction rate and freezing of water at low temperatures. The use of alcohol instead of water as an alternative to the production of H_2 from $NaBH_4$ is being evaluated by researchers such as methanol [3,8–10], ethanol [11,12], ethylene glycol [13] and propylene glycol [14]. From the interaction of alcohols with $NaBH_4$ as a solvent to the production of H_2 by the hydrolysis of $NaBH_4$, it has superior features such as use at low temperatures, simpler regeneration processes and faster reaction kinetics [16]. Therefore, it would be beneficial to further study alcohols for efficient H_2 production from $NaBH_4$.

Methanol, consisting of a methyl group attached to a polar hydroxyl group, is the simplest aliphatic alcohol and is a light, volatile, colourless, flammable liquid with a distinctive alcoholic odour. Methanol, which is produced in more than 20 million tons per year, is used as a precursor of acetic acid, formaldehyde, methyl benzoate, methyl tert-butyl ether as well as other commercial chemicals [15]. Ethylene glycol, which is completely miscible with water and many organic liquids, can be used in a wide variety of reactions with its hydroxyl groups as a colourless and odourless organic solvent widely used as antifreeze in heating and cooling systems [16]. There are very limited studies on the production of H_2 from the $NaBH_4$ ethylene glycolysis reaction [13,17]. This study will contribute to the literature.

The H_2 production reactions of $NaBH_4$ methanolysis and ethylene glycolysis reactions are given below, respectively.

$$NaBH_4 + 4\ CH_3OH \rightarrow 4\ H_2 + NaB\ (OCH_3)_4 \quad (1)$$

$$NaBH_4 + 2\ CH_2OHCH_2OH \rightarrow 4\ H_2 + NaB\ (OCH_2)_4 \quad (2)$$

As with $NaBH_4$ hydrolysis, it is important to use a suitable and effective catalyst for the rapid and optional production of H_2 from $NaBH_4$ in methanol or ethylene glycol. Various homogeneous and heterogeneous active non-metallic catalysts have been reported for $NaBH_4$

E-mail address: sakaca1976@gmail.com.

https://doi.org/10.1016/j.apcatb.2022.122335
Received 21 October 2022; Received in revised form 25 December 2022; Accepted 27 December 2022
Available online 28 December 2022

methanolysis. Among these homogeneous catalysts, acid catalysts showed a fast hydrogen production rate by supporting proton formation for $NaBH_4$ methanolysis. However, catalyst regeneration becomes difficult due to the high solubility in methanol. To overcome this, nanoparticles, usually based on acid-treated carbon materials, have been investigated for $NaBH_4$ methanolysis [18–21]. Despite their high activities, metal-based catalysts, which have cost and environmental disadvantages, have been used in such reactions and continue to be used [9,10,22,23]. Metal-free catalysts have superior advantages over metal-based catalysts such as environmental friendliness, stability of catalytic activity, and better performance in terms of cost. Therefore, there is a need to develop new metal-free catalysts with both high catalytic performance and low cost.

In recent years, the direct use of environmentally friendly and economical natural compounds for catalytic applications has become an important strategy. Of these natural compounds, biopolymers have an important place, especially in various heterogeneous catalytic systems. These cost-effective and widely abundant biopolymers have free alcoholic and amine groups that enable the activation of both nucleophiles and electrophiles through interactions such as ion pairs and hydrogen bonding. These biopolymers are widely preferred among raw materials due to their chitosan, natural element nitrogen, low price and good biocompatibility [24]. Chitosan, which has up to 10 billion tons of biological reserves on earth, allows mechanical and chemical modifications with abundant functional groups in its structure. Chitosan, which contains functional groups such as hydroxyl and amino and is the second most abundant natural polymer after cellulose, is widely used in different applications and is a natural organic polymer with biodegradable features [25–28]. Chitosan, whose main monomeric unit is the N-glucosamine moiety, can both act as a catalyst and support the synthesis of catalysts [26,29]. Amine and hydroxyl groups, which have lone electron pairs in the structure of chitosan, can offer electron-rich reactive sites for various applications [26]. Chitosan's insolubility in most solvents, flexibility, and ability to absorb species such as metals make it an outstanding heterogeneous catalyst [30]. Chitosan's abundant hydroxyl and amine groups offer unique surface chemistry for various cross-links with macromolecules, metal ligands and ionic species through various bonding [31].

Zeolites, a natural aluminosilicate mineral that can be used in various applications such as separation, purification, catalysis and adsorbents, are also an important inorganic material [32,33]. Clinoptilolite from the Heulandite group, which is the most widely used in environmental and industrial applications, is widely used in catalytic applications [34]. The acidic properties of zeolites are important in catalytic applications due to the Brønsted acid in their structure and some cases additionally Lewis acid regions [35].

However, mass transfer and diffusion of macromolecular reactants and products, especially at low temperatures, are negatively affected by microporous zeolite channels [36]. The textural and acidic properties of microporous zeolites can be adjusted appropriately by acid modification [37–40]. The mechanical, thermal and chemical properties of the hybrid composite material formed by the combination of recyclable and/or non-toxic inorganic zeolites and organic chitosan can be improved [41]. Zeolite/chitosan composites have been used successfully in various applications [42]. Replacing zeolite frameworks with cross-linked chitosan results in a material with superior surface area and efficiency. The hybrid combination of chitosan and zeolite crystals simultaneously elevated the properties of both materials, making them a more practical material for more sophisticated applications [43]. The solubility, hydrophobicity, mechanical stability and chemical stability properties of chitosan can be improved in acidic media by the cross-linking reaction used to improve the physicochemical properties of chitosan [44].

One of the important modification steps for catalytic reactions is the protonation process. H_2 production can be improved faster by promoting the adsorption of positively charged species formed by protonation on the chitosan-zeolite hybrid composite surface and ions such as alkoxide and BH_4^- in the $NaBH_4$ methanolysis and $NaBH_4$ ethylene glycolysis medium to the catalyst surface [45,46].

In this study, the synthesis of low-cost, non-toxic and recyclable zeolites and chitosan hybrid composite metal-free catalysts and the protonation process using hydrochloric acid of the obtained catalysts by hydrothermal heating were carried out. One of the unique aspects of this study is that chitosan-zeolite composites, which are generally used for the removal of pollutants from aqueous solution, were used for the first time in the production of H_2 from $NaBH_4$ methanolysis and $NaBH_4$ ethylene glycolysis reactions. Another unique aspect of this study is the use of the material obtained by protonating both zeolite and chitosan simultaneously with hydrochloric acid in the production of H_2. At the same time, the obtained protonated chitosan-zeolite hybrid catalysts are discussed in detail for the first time to produce H_2 from $NaBH_4$ methanolysis and ethylene glycol reactions. The prepared chitosan-zeolite-H composite was characterized by XRD, SEM-EDS, FTIR, TEM and XPS analyses. Also, the possible mechanism of H_2 formation in methanol and ethylene glycol with chitosan-zeolite-H is discussed.

2. Experimental section

Natural clinoptilolite zeolite was obtained from a commercial company (Rota Mining Corp., Turkey). The chitosan powder was purchased from a commercial company (Nurbal, Turkey). Methanol (99.8%, Tekkim, Turkey), ethylene glycol (Merck, Germany), $NaBH_4$ (96%, Merck, Germany) and HCl (37%, Merck, Germany) are of analytical purity and no extra treatment was performed.

2.1. Sample preparation

Metal-free hybrid chitosan/zeolite-based catalysts were synthesized in two steps. The first stage is the calcination process of chitosan and zeolite. For this purpose, different chitosan/zeolite ratios (1:0.25, 1:0.5, 1:1 and 1:1.5) and different calcination temperatures (200, 300, 400 and 500 °C) were used. Air was used during the calcination process. The calcination time was applied as 60 min. H_2 values obtained from $NaBH_4$ methanolysis were used to determine the most suitable catalyst. After the optimum ratio and calcination temperature were determined, the second stage of the study was started. At this stage, hydrothermal protonation was applied with hydrochloric acid in a magnetic stirrer at 50 °C for 6 h. For optimum hydrochloric acid concentration, the acid/water ratio was applied as 1:1, 1:2, 1:3 and 1:4. The samples obtained after acid activation was first washed with distilled water and then dried for 4 h in an oven at 70 °C. The hybrid catalyst obtained in the first step was labelled chitosan/zeolite, and the hybrid catalyst obtained in the second step was labelled chitosan-zeolite-H.

2.2. Characterization

Surface morphological properties of raw chitosan and chitosan/zeolite-H composites were investigated with an SEM (Carl Zeiss EVO 18 model) and energy dispersive X-ray spectrometry (EDS).

The chemical compositions and conditions of raw chitosan and chitosan-zeolite-H catalysts were investigated with XPS (Escalab 250Xi, Thermo Fisher Co., USA).

An XRD device (PANalytical Empyrean) with Cu Ka radiation (λ = 1.54056 Å) in the range of 10–80° was used for the changes in the crystal structure of the same samples.

Surface functional groups of hybrid composites were examined in the wavelength range of 4000–400 cm^{-1} with the ATR-FTIR device (Bruker, Germany).

The nanoscale images of raw chitosan and chitosan-zeolite-H catalysts were examined with a JEM-2100 F (JEOL) model TEM.

BET surface area and pore size distributions of metal-free catalysts were measured at 77 K with N_2 adsorption/desorption isotherms (Micromeritics ASAP 2460 instrument). The degas treatment of the

samples was carried out at 100 °C for 3 h.

2.3. H_2 production and reusability

Experimental studies on the production of H_2 from $NaBH_4$ methanolysis and $NaBH_4$ ethylene glycolysis reactions with chitosan-zeolite-H hybrid metal-free catalysts were carried out with a flat-bottom flask placed in a thermostated water bath. To this reaction flask, first, a certain amount of $NaBH_4$ was added, followed by 10 mg of catalyst. Next, either methanol (10 ml) or ethylene glycol (10 ml) was injected into this reaction vial with a syringe. The volume of H_2 obtained by water displacement was recorded using a graduated measuring tape. Theoretically, 50% of the H_2 volume was taken into account in calculating the HGR value. The effect of temperature (15, 20, 30, 40 and 50 °C), the effect of $NaBH_4$ (0.125 g, 0.25 g, 0.375 g and 0.5 g) and reusability parameters on H_2 production were discussed. Reusability experiments were repeated five times in succession.

3. Results and discussion

3.1. Characterization studies

XRD diffractograms of raw chitosan, raw zeolite, chitosan-zeolite and chitosan-zeolite-H composites are shown in Fig. 1. The XRD diffractogram of raw chitosan gives a peak at 2θ: 19.8°. The diffraction peaks in the XRD pattern at 2θ = 11.18°, 13.04°, 17.32°, 19.08°, 20.42°, 22.35°,23.88°, 25.99°, 28.11°, 29.47°, 31.97° and 36.86° for the raw zeolite can be interpreted as typical characteristics of the clinoptilolite structure [47,48]. The XRD patterns observed for chitosan-zeolite composites mainly show zeolite peaks. However, the peak intensities of the raw zeolite were weakened by the dispersion of chitosan on the zeolite crystals. This result can be interpreted as the interaction between chitosan and zeolite. Compared to the chitosan-zeolite composite, the peak in chitosan was lost due to the significant structural changes during the composite formation. The disappearance of this peak has been explained due to the high intercalation between zeolite and chitosan [49]. However, there are significant changes in the XRD pattern obtained after the interaction of the chitosan-zeolite composite with hydrochloric acid. At the same time, some peaks were lost for zeolite as a result of interaction with hydrochloric acid and chitosan. The average crystallite sizes calculated from the Scherer equation for the raw zeolite, chitosan-zeolite and chitosan-zeolite-H composites were 14.10 nm, 12.09 nm, and 1.88 nm, respectively. The crystallinity of the chitosan-zeolite-H composite was lower compared to the raw zeolite, chitosan-zeolite composites.

Fig. 2 shows SEM images of raw zeolite (a, b), raw chitosan (c, d) chitosan-zeolite (e, f), and chitosan-zeolite-H (g, h) composites. Fig. 2a, b shows the raw zeolite clinoptilolite micromorphological features. As

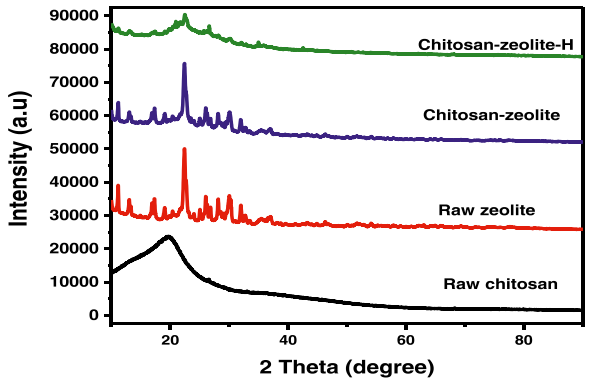

Fig. 1. XRD diffractograms of raw chitosan, raw zeolite, chitosan-zeolite and chitosan-zeolite-H composites.

shown in the figure, zeolite clinoptilolite has a surface with partially developed crystalline laminar and conglomerates of compact crystals. It was observed that the surface morphology of raw chitosan (Fig. 2c, d) was smooth and slightly porous. The surface morphology of the chitosan-zeolite composite (Fig. 2e, f) was different from that of both natural zeolite and chitosan. The fact that the zeolite crystals cannot be seen clearly during the formation of the composite with chitosan molecules can be interpreted as the successful formation of the zeolite and chitosan composite. The SEM image of the chitosan-zeolite-H composite (Fig. 2g, h) shows that both the chitosan becomes more porous with hydrochloric acid and the zeolite is uniformly dispersed in the chitosan matrix with a layered structure. Fig. 3 shows TEM images of raw chitosan (a), raw zeolite (b), chitosan-zeolite(c), and chitosan-zeolite-H (d) composites. Similar to SEM images, the surface morphology of raw chitosan (Fig. 3a) was observed to be smooth and uniform. As seen in Fig. 3(b), the raw zeolite crystal has a spherical and agglomerated layered structure, with an approximate particle size of 18.62 nm. TEM images for zeolite-chitosan revealed a block-like layered surface with an approximate particle size of 13.45 nm (Fig. 3c). The TEM image of the chitosan-zeolite-H composite (Fig. 3d) shows that the zeolite is homogeneously dispersed in the chitosan matrix. The average size of the chitosan-zeolite-H composite was 1.24 nm. The particle sizes obtained after hydrochloric acid treatment decreased, consistent with the average crystallite size values observed by XRD patterns. This means that activation with hydrochloric acid has a positive effect on forming smaller active phase particles on the surface. Due to the deterioration of the structure of the zeolite as a result of the decrease in particle size, the collapse of the voids and a decrease in the specific surface area are in question [50]. Table 1 confirms that the surface area of the zeolite is reduced. The particle size reduction of the zeolite in the acid-treated chitosan-zeolite composite may be the result of the partial dissolution of the octahedral layer and fracture of the middle or side layers under the influence of high shear forces. Similarly, this result was obtained when the clay sample was treated with acid [51]. The dispersibility of zeolite particles on chitosan increased significantly with acid treatment. In the literature, there is a similar situation with acid treatment on clay-structured catalysts [52].

Fig. 4 shows the EDS for the raw zeolite, raw chitosan, chitosan-zeolite, and chitosan-zeolite-H (e, f) composites. The presence of C, O, N, Al and Si atoms as the main components of the chitosan-zeolite and chitosan-zeolite-H composite shows that the chitosan and zeolite composite composition was formed successfully. The weight percentages for the C, N and O elements for raw chitosan were found to be 41%, 73%, 0.23%, and 58.03%, respectively. The weight percentages for the C, N, O, Al and Si elements for the chitosan-zeolite were found to be 51.39%, 4.23%, 36.07%, 1.20%, and 7.11%, respectively. For the chitosan-zeolite-H composite, the weight percentages corresponding to the C, N, O and Si elements were found to be 56%, 4.06%, 27.58% and 5.71%, respectively. As can be understood, although Al was present in the raw zeolite and the chitosan-zeolite composite, the Al element was not found in the chitosan-zeolite-H composite, possibly due to dealumination by interaction with hydrochloric acid. At the same time, the EDS results for the chitosan-zeolite-H composite showed that chlorine atoms were also present in the structure due to the treatment with hydrochloric acid.

FTIR spectra of raw zeolite, chitosan, chitosan-zeolite, and chitosan-zeolite-H composites are shown in Fig. 5. The peak at about 3358 cm^{-1} for raw chitosan is due to the vibration of the OH-hydroxyl groups. C–H bands were observed at approximately 2872 cm^{-1} [53]. For raw chitosan, C-O vibrations at approximately 1647 cm^{-1} and C-N vibrations at approximately 1413 cm^{-1} were observed. The peaks observed between 1151 cm^{-1} and 889 cm^{-1} were attributed to vibrations of the glycosidic bonds, C–O and C–O–C stretching vibrations [54]. In the FTIR spectrum of the crude zeolite clinoptilolite sample, peaks are intense at 450–1750 cm^{-1}. It originates from the peak heulandite phase that occurs at approximately 593 cm^{-1} [55]. For the raw zeolite, FTIR bands in the range of 1200–400 cm^{-1} are attributed to internal tetrahedral Si-O

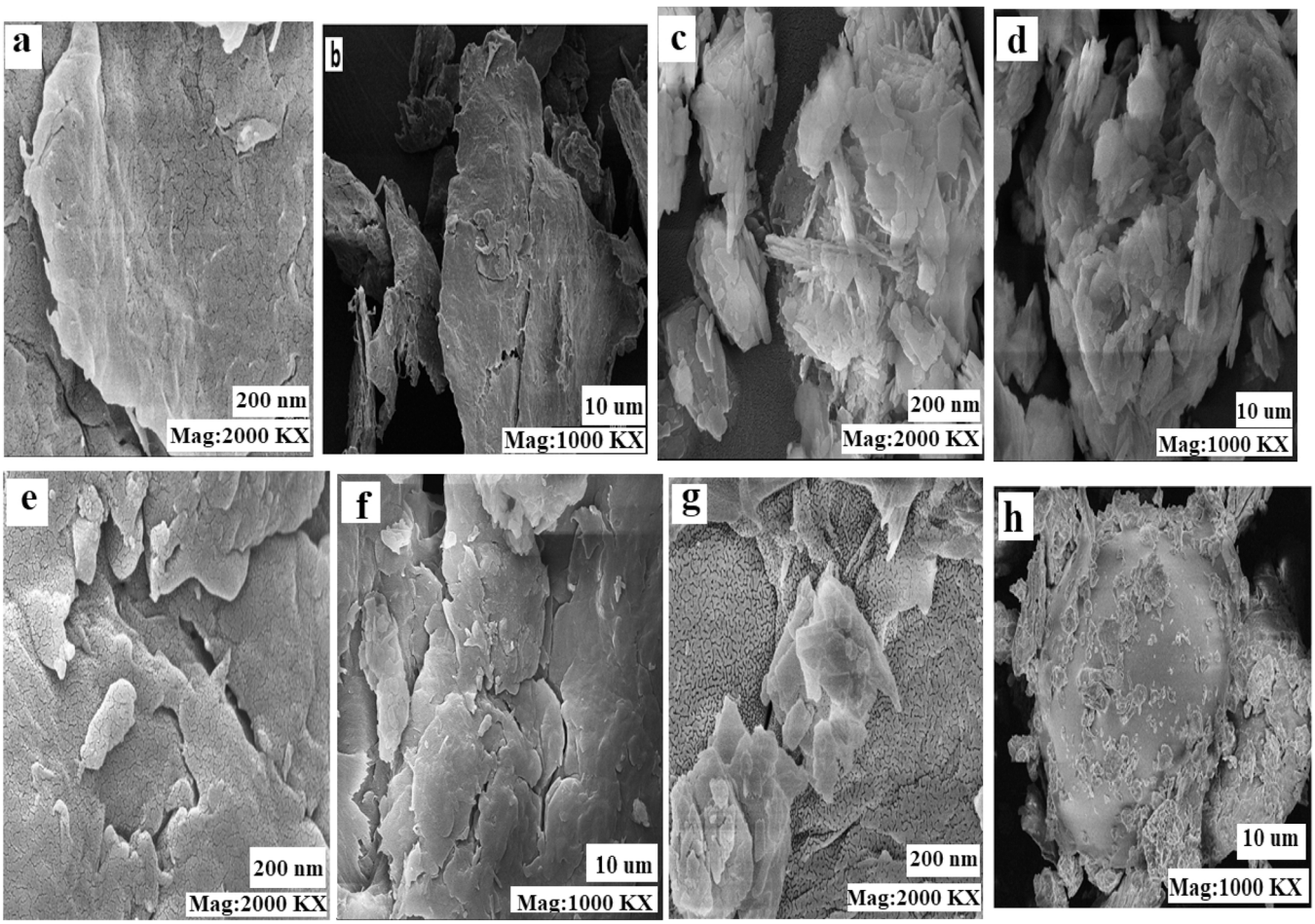

Fig. 2. SEM images of raw zeolite (a, b), raw chitosan (c, d) chitosan-zeolite (e, f), and chitosan-zeolite-H (g, h) composites.

(Si) and Si-O (Al) vibrations with silico- and alumina-oxygen bridges [56]. The peaks belonging to both zeolite and chitosan species can be seen in the FTIR spectrum of the zeolite-chitosan composite. The positively charged amino (NH_3^+) group is seen at approximately 1540 cm^{-1} in the zeolite-chitosan composite [49]. The FTIR spectrum for chitosan-zeolite-H demonstrates the successful integration between chitosan and zeolite. The spectrum observed for chitosan-zeolite-H, Si–O–Si peaks at 983.4 cm^{-1} can be attributed to the presence of zeolite in the composite structure. C–O peaks at approximately 1067 cm^{-1} and N–H peaks at 1602 cm^{-1} can be interpreted as the presence of chitosan in the structure. The formation of chitosan and zeolite composites may be related to the electrostatic interaction observed between the negatively charged regions (SiO^-) and NH_3^+ groups [57]. Compared to raw chitosan, there is a decrease in the peak intensity of the composite at 1652 and 1420 cm^{-1} due to complex reactions [58]. On the other hand, the intensity of the absorption bands of NH_2 (about 1602 cm^{-1}) in chitosan decreased due to the formation of composite with zeolite and interaction with hydrochloric acid. This result can be interpreted as hydrogen bond interactions between chitosan and zeolite and interactions between the NH_2 of chitosan and the OH of the zeolite [59,60]. At the same time, the decrease in peak density around 1600 cm^{-1} of the catalyst sample can be interpreted as a successful protonation process [61]. As a result of the interaction with hydrochloric acid, the band from about 1030 cm^{-1} for raw chitosan shifted to 1060 cm^{-1}. Also, the band at about 1080 cm^{-1} for chitosan-zeolite-H can be attributed to the Si–O–Si anti-symmetric tensile vibration [48].

N_2 adsorption-desorption isotherms (a) and BJH pore radius distributions(b) of raw chitosan, raw zeolite, chitosan-zeolite and chitosan-zeolite-H composites are shown in Fig. 6 and Table 1 give the obtained values. BET surface area values obtained for raw chitosan, raw zeolite, chitosan-zeolite and chitosan-zeolite-H were found to be 1.11, 33.69, 8.31 and 7.58 m^2g^{-1}, respectively. As can be understood, the surface area of the chitosan-zeolite composite decreased due to the coating of the pores of the raw zeolite with chitosan. This result can support the formation of the composite structure. At the same time, there is an increase in the BET surface area after the interaction of the chitosan-zeolite composite with hydrochloric acid, possibly due to the opening of the pores by the acid. The pore radius values given in Table 1 vary between 1.5 and 2. According to the classification accepted by the International Union of Pure and Applied Chemistry, these samples are in the micropore structure according to their pore diameters. Understandably, BET surface areas are low for all samples. However, as can be seen in the FTIR spectrum, there are more distinct functional groups for the chitosan-zeolite-H composite. These functional groups are active for H_2 production from $NaBH_4$ methanolysis and $NaBH_4$ ethylene glycolysis reactions.

Fig. 7 shows the XPS analysis of raw chitosan and chitosan-zeolite-H samples. XPS spectrum of the chitosan-zeolite-HCl sample confirmed the presence of C(52.14), N(3.14%), O(31.33) and Si(13.37). The presence of Si and N atoms is an indication of the successful formation of a hybrid structure containing zeolite and chitosan. Also, the XPS spectrum for the raw chitosan sample confirmed the presence of C(62.4%), N(6.17%) and O(30.72). The obtained weight percentages of the elements are compatible with the EDS analysis.

High-resolution spectra of the chitosan-zeolite-H sample for C 1 s, N1s, Si 2p and O1s are shown in Fig. 8a, b, c and d. Fig. 7a shows the binding energies of the C1s spectrum at 282.07 eV (C–N/O–C–O),

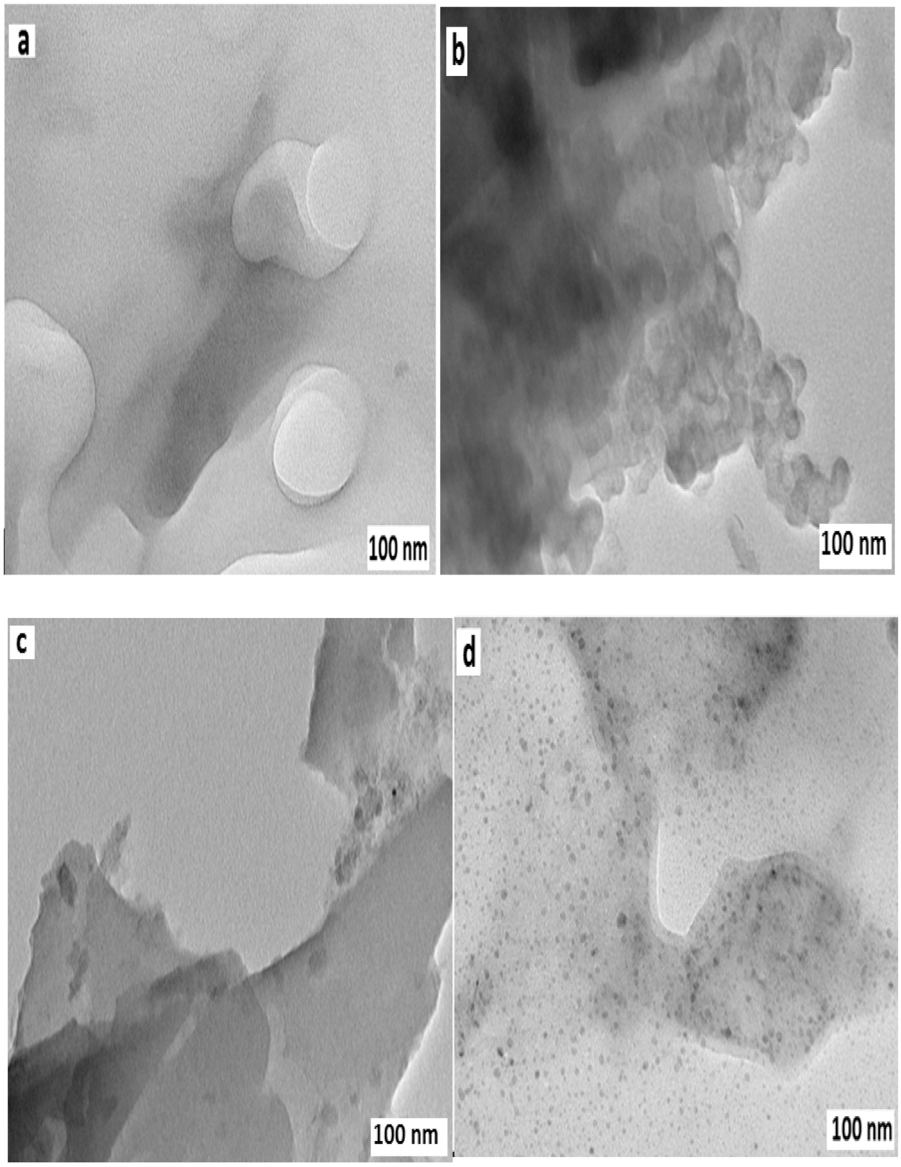

Fig. 3. TEM images of raw chitosan (a) raw zeolite (b), chitosan-zeolite(c), and chitosan-zeolite-H (d composites.

Table 1
Surface properties for raw chitosan, raw zeolite, chitosan-zeolite and chitosan-zeolite-H composites.

	Pore radius (nm)	Pore volume (cc/g)	BET surface area (m^2g^{-1})
Zeolite	1.527	0.072	33.69
Chitosan	1.529	0.002	1.11
Chitosan-zeolite	1.910	0.030	8.31
Chitosan-zeolite-H	1.931	0.013	7.58

284.35 (C−C/C═C) and 287.9 (C−OH) eV, respectively [62,63]. N1s high-resolution XPS spectra of the chitosan-zeolite-H sample are shown in Fig. 7b. A peak at 402.1 eV was interpreted to ammonium form (NH_3^+) by N1s deconvolution of the chitosan-zeolite-H sample [64]. This result can be interpreted by the bonding of hydrogen atoms to the structure with hydrochloric acid. A similar situation was observed in the FTIR spectrum. The peaks observed at binding energies of 397.28 and 397.66 eV in the chitosan-zeolite-H sample were interpreted as C-NC sp^2-bonded N atoms and tertiary $(N-(C)_3)$ groups, respectively [65]. In

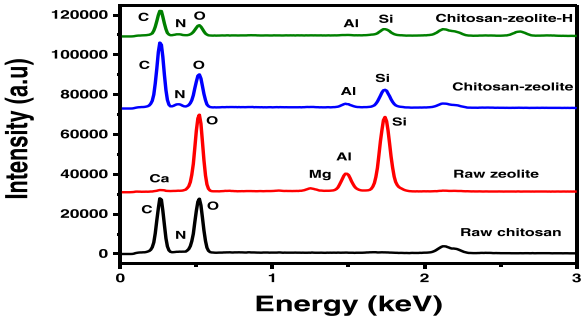

Fig. 4. EDS for the raw zeolite, chitosan, chitosan-zeolite, and chitosan-zeolite-H composites.

addition, the N1s peak at 397.66 eV can be attributed to the Si–N coupling phase [66]. In the spectrum of the chitosan-zeolite-H sample, there are two characteristic peaks for O1s at binding energies of 529.98 eV and 531.05 eV. The O1s peaks at 531.05 eV can be attributed to the N-C-O chemical bonds in the N-acetylated-glucosamine units

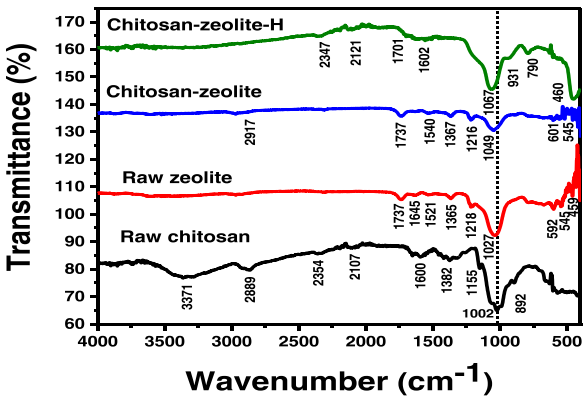

Fig. 5. FTIR spectra of raw zeolite, raw chitosan, chitosan-zeolite, and chitosan-zeolite-H composites.

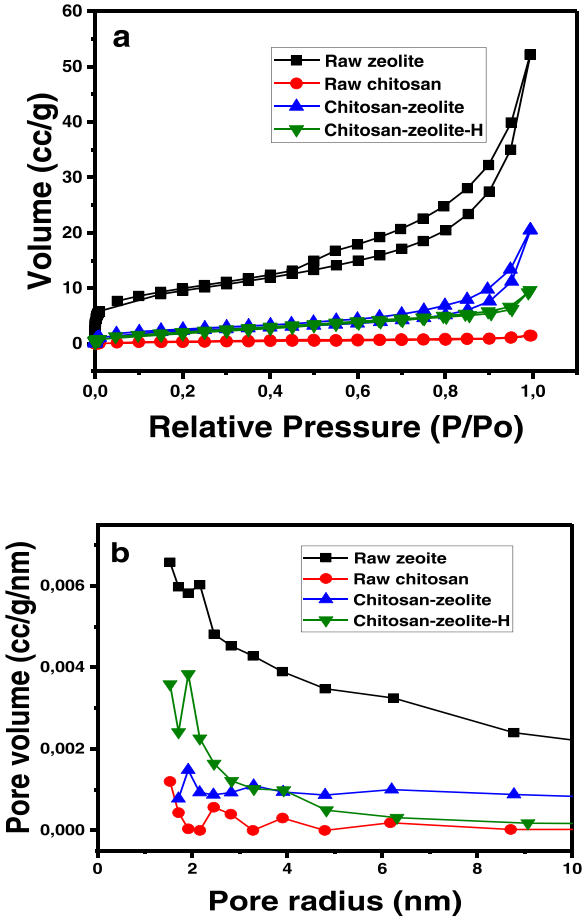

Fig. 6. N_2 adsorption-desorption isotherm(a) and Pore size distributions (b) of raw chitosan, raw zeolite, chitosan-zeolite and chitosan-zeolite-H composites.

[67].

3.2. Hydrogen production studies

The effect of temperature (200, 300, 400 and 500 °C) on chitosan and zeolite hybrid material was investigated at a 1:1 chitosan-zeolite ratio (Fig. 9). The hybrid material obtained after heat activation was used as a catalyst in the production of H_2 from $NaBH_4$ methanolysis at 30 °C. The HGR values obtained with the hybrid material obtained at 200, 300, 400 and 500 °C temperatures were found as 3500, 3700, 3400

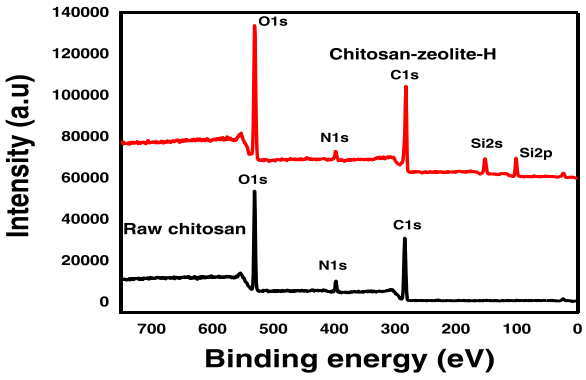

Fig. 7. XPS analysis of raw chitosan and chitosan-zeolite-H samples.

and 3300 ml $min^{-1}g^{-1}$, respectively. As can be understood, the best HGR value was obtained with chitosan/zeolite activated at 300 °C. According to Ismadji et al. [68] stated that the optimum temperature for heat activation on zeolite is 300 °C. They stated that the efficiency decreased by about 18% at temperatures above 300 °C. In this study, 300 °C was used as the optimum temperature.

Fig. 10 shows the effect of the chitosan-zeolite ratio on chitosan and zeolite hybrid material. Also, Fig. 10 shows the time-dependent H_2 production volumes in the raw zeolite, raw chitosan, and only methanol. This $NaBH_4$ reaction with only methanol was completed in approximately 15 min. The completion times of this reaction with raw chitosan and raw zeolite in methanol were found to be 15 and 14 min, respectively. As can be understood, chitosan in methanol did not contribute to H_2 production, while raw zeolite contributed very little. The acidic nature of the methanol reaction affects the catalytic performance. The methanol reacts with the sodium ion of $NaBH_4$ to form alkoxide. These reactions of alcohols can be an indication of their acidic nature. The acidic structure resulting from the proton in the hydroxyl groups of alcohols weakens due to the increase in the electron density of the oxygen atom by adding an electron-donating group to this hydroxyl group. The ratios of 1:0.25, 1:0.5, 1:1, and 1:1.5 for the chitosan/zeolite were used. HGR values from $NaBH_4$ methanolysis by 1:0.25, 1:0.5, 1:1, 1:1.5 for the chitosan/zeolite ratio obtained were found as 4000, 4500, 3700, and 3400 ml $min^{-1}g^{-1}$, respectively. Also, the completion times of $NaBH_4$ methanolysis by the ratio of 1:0.25, 1:0.5, 1:1, and 1:1.5 for the chitosan/zeolite were 9, 8, 10, and 11 min. As can be understood, the best chitosan/zeolite ratio was determined as 1:0.5. The completion times of this reaction with only methanol, raw chitosan and raw zeolite in methanol were found to be 15, 15 and 14 min, respectively. Compared to raw chitosan, raw zeolite and only methanol, there is an improvement of approximately 45–50% in the catalytic activity with the 1.0.5 chitosan/zeolite hybrid catalyst. These results showed that the chitosan/zeolite hybrid material provided a significant improvement in catalytic activity. There is a decrease in the HGR values obtained depending on the increase in the amount of zeolite. Probably, the particles in this methanolysis reaction could not find a suitable active site on the catalyst surface to produce H_2 due to the increase in the zeolite ratio.

In this study, hydrochloric acid was used for the protonation of chitosan-zeolite hybrid composites. The acid concentration of 1:1, 1:2, 1:3 and 1:4 acid/water ratio was applied to the chitosan-zeolite hybrid composite. At the same time, hydrochloric acid was applied to both the raw zeolite and the raw chitosan at a 1:1 acid/water ratio. Fig. 11 shows the H_2 production volumes from $NaBH_4$ methanolysis with hydrochloric acid-treated raw zeolite, raw chitosan, and chitosan/zeolite hybrid composites. The HGR values obtained with the acid/water ratio 1:1, 1:2, 1:3 and 1:4 were found to be 6600, 5333, 4750, and 4500 ml $min^{-1}g^{-1}$, respectively. There is a decrease in HGR values depending on the increase in the dilution ratio. At the same time, HGR values obtained with raw zeolite and raw chitosan treated with a 1:1 acid/water ratio were

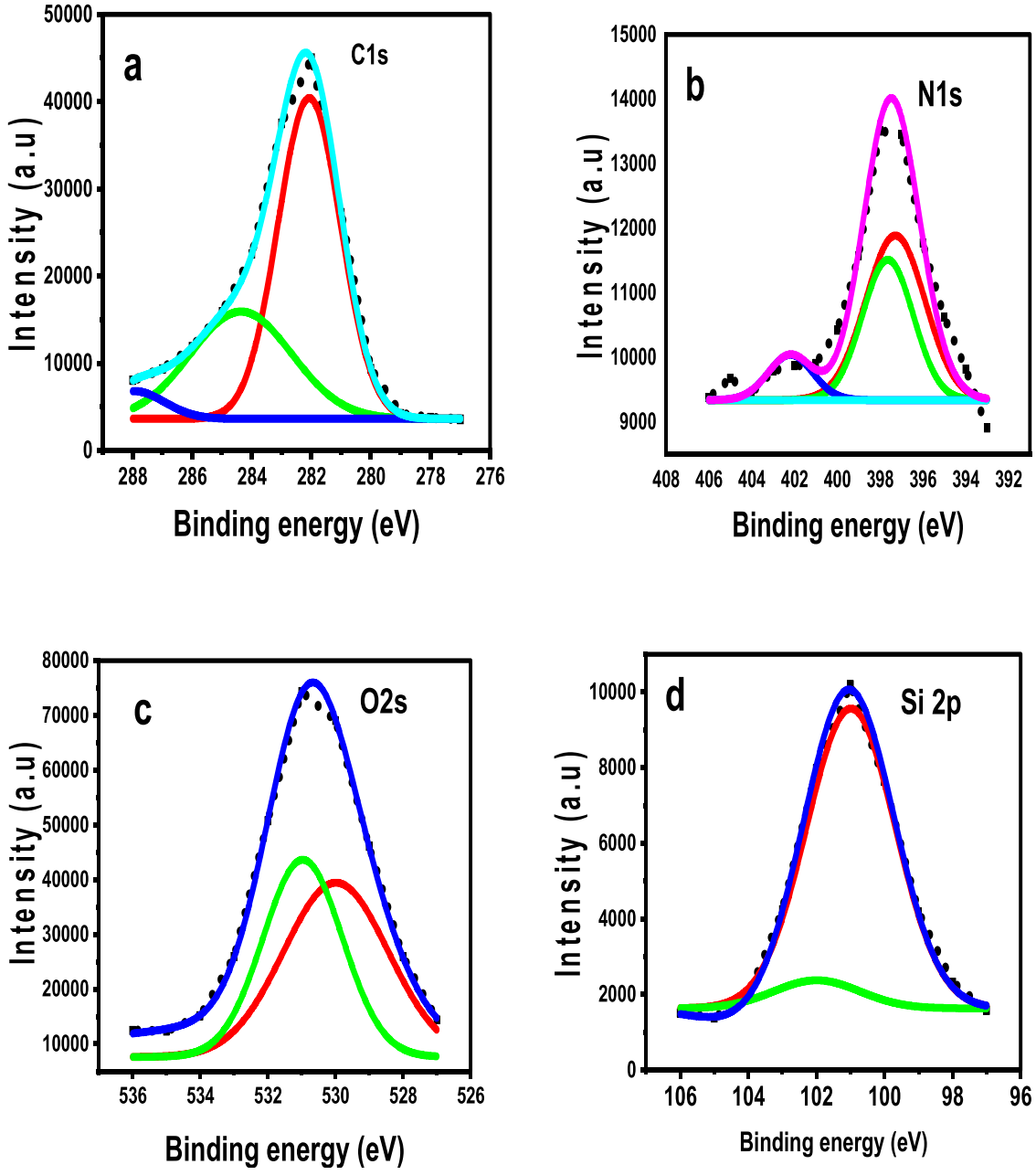

Fig. 8. High-resolution spectra of the chitosan-zeolite-H sample for C 1 s(a), N1s(b), Si 2p(c) and O1s(d).

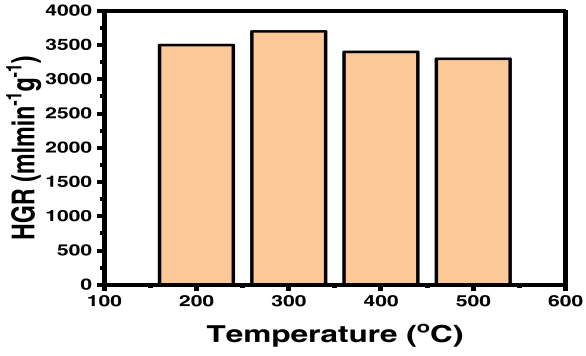

Fig. 9. The effect of temperature (200, 300, 400 and 500 °C) on chitosan and zeolite hybrid material at a 1:1 chitosan-zeolite ratio.

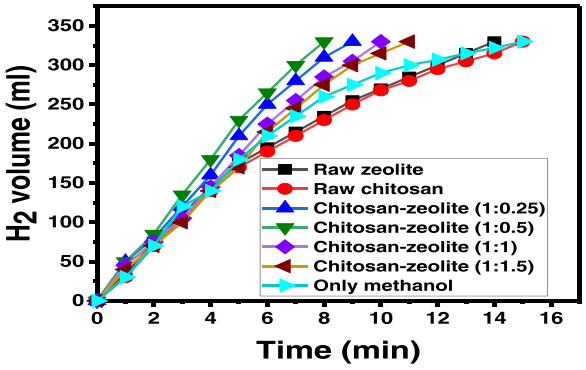

Fig. 10. Effect of the chitosan-zeolite ratio (1:0.25, 1:0.5, 1:1, 1:1.5) and the raw zeolite, raw chitosan, and only methanol on the H_2 production volumes.

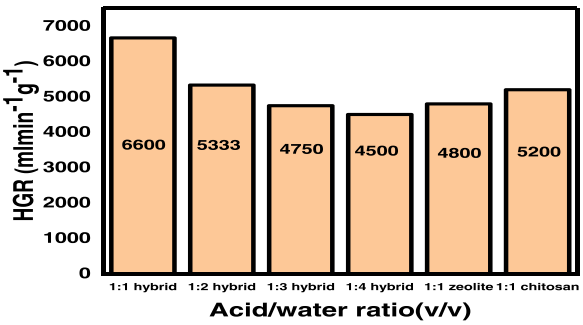

Fig. 11. H_2 production volumes from $NaBH_4$ methanolysis with hydrochloric acid-treated chitosan/zeolite hybrid composites by the acid/water ratio of 1:1, 1:2, 1:3, 1:4 and the raw zeolite and the raw chitosan at a 1:1 acid/water ratio.

found to be 4800 and 5200 ml $min^{-1}g^{-1}$, respectively. These results show that the protonation of this hybrid catalyst has a significant effect on H_2 production from $NaBH_4$ methanolysis.

Fig. 12a and 12b show the effect of $NaBH_4$ concentrations (0.125, 0.25, 0.375 and 0.5 g) on H_2 production by $NaBH_4$ methanolysis and $NaBH_4$ ethylene glycolysis reactions, respectively, with 10 mg of chitosan-zeolite-H at 30 °C. As can be seen from the figures, $NaBH_4$ concentrations have a similar effect on H_2 production from methanolysis and ethylene glycolysis reactions. HGR values of 6666, 17,500, 25,000 and 28,666 ml $min^{-1}g^{-1}$ were obtained from the methanolysis reaction with 0.125, 0.25, 0.375 and 0.5 g $NaBH_4$, respectively. Also, TOF values obtained from the methanolysis reaction with 0.125, 0.25, 0.375 and 0.5 g $NaBH_4$ were 115, 307, 438, and 552 h^{-1}, respectively. HGR values of 5666, 10,428, 18,000 and 27,333 ml $min^{-1}g^{-1}$, respectively, were obtained from the reaction of ethylene glycolysis with the same amounts of $NaBH_4$. Also, TOF values obtained from the ethylene glycolysis reaction with 0.125, 0.25, 0.375 and 0.5 g $NaBH_4$ were 99, 175, 315, and 456 h^{-1}, respectively. By increasing the amount of $NaBH_4$ from 0.125 g to 0.25 g, there is an approximately three-fold increase in the HGR value obtained from the methanolysis reaction, while there is an approximately two-fold increase in the ethylene glycolysis reaction. However, by increasing the amount of $NaBH_4$ from 0.25 g to 0.5, there is a 1.6 and 2.6-fold increase in the HGR increase rates obtained from the methanolysis and ethylene glycolysis reactions, respectively. These results show that methanol as a solvent is effective in low $NaBH_4$ amounts and ethylene glycol is effective in high $NaBH_4$ amounts in the production of H_2 from the $NaBH_4$ reaction. In response to the increase in the amount of $NaBH_4$ due to the reaction progress, there is a decrease in the increase of the HGR value with decreasing methanol in the solution medium. In contrast, the slow kinetics of ethylene glycol at the start of the reaction compared to methanol tends to increase with time. Thus, higher HGR values are obtained with an increasing amount of $NaBH_4$.

The values of 1.07 and 1.12 obtained from the slope of the logarithmic plot of the concentration of $NaBH_4$ versus the rate of HGR in methanol and ethylene glycol, respectively, indicate that these catalytic reactions are first-order versus $NaBH_4$.

The effect of temperature on the production of H_2 from $NaBH_4$ methanolysis and ethylene glycolysis reactions was examined using 10 mg chitosan-zeolite-H and 0.125 g $NaBH_4$ with temperature values in the range of 15–50 °C, and the resulting H_2 volumes are given in Fig. 13a and 13b. The higher the temperature, the less time it took for the reaction to complete. As can be understood, the temperature effect on both reactions gave similar shapes. For the $NaBH_4$ methanolysis reaction, HGR values of 3400, 3800, 6666, 13,333 and 17,000 ml $min^{-1}g^{-1}$ were obtained for the temperatures of 15, 20, 30, 40 and 50 °C, respectively. In contrast, the HGR values obtained for the $NaBH_4$ ethylene glycolysis reaction for the same temperature values were 1500, 2750, 5666, 9000 and 12,666 ml $min^{-1}g^{-1}$, respectively.

Ea values were calculated from the Arrhenius equation (Eq. (3)) for the chitosan-zeolite-H catalyzed $NaBH_4$ methanolysis and ethylene glycolysis reactions.

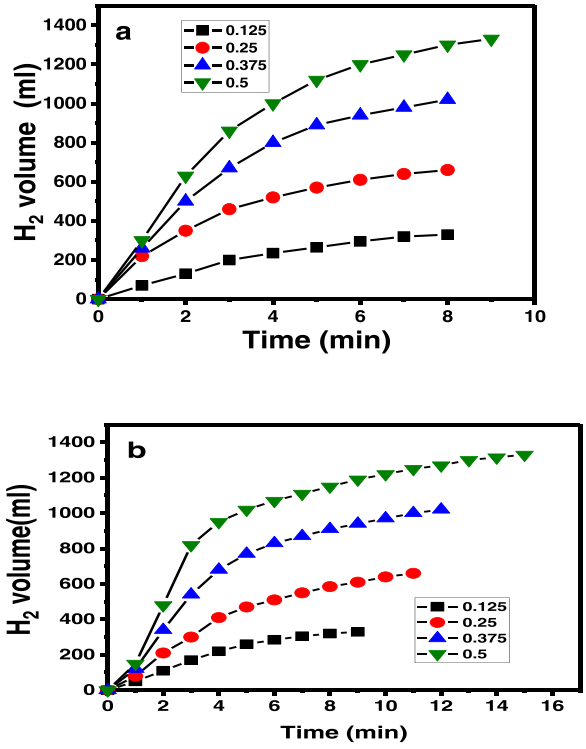

Fig. 12. Effect of $NaBH_4$ concentrations (0.125, 0.25, 0.375 and 0.5 g) on H_2 production by $NaBH_4$ methanolysis (a) and $NaBH_4$ ethylene glycolysis (b) reactions.

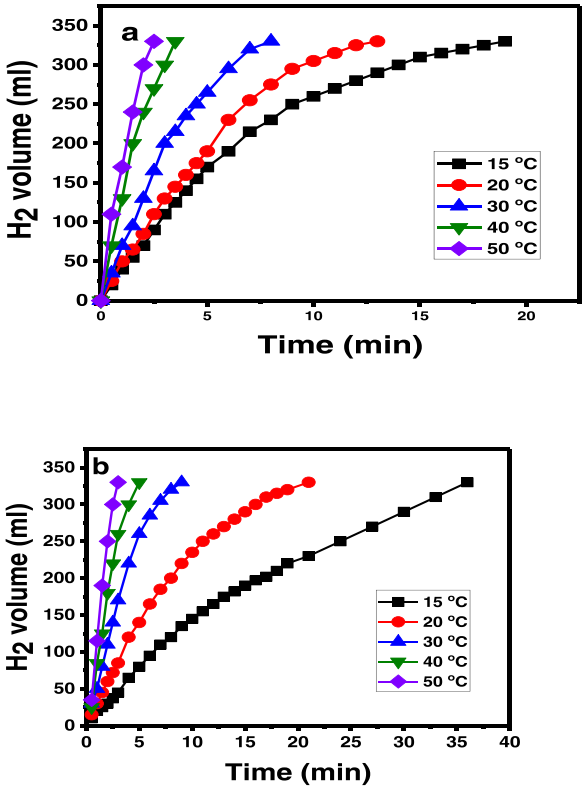

Fig. 13. Effect of temperature on the production of H_2 from $NaBH_4$ methanolysis(a) and ethylene glycolysis(b) reactions using 10 mg chitosan-zeolite-H and 0.125 g $NaBH_4$.

$$\ln k = \ln A - Ea / RT \quad (3)$$

where k is the rate constant of the methanolysis and ethylene glycolysis reactions, R is the gas constant, A is the pre-exponential factor, and T is the reaction temperature in Kelvin. Fig. 14a and 14b give the Arrhenius plots obtained at different temperatures for the $NaBH_4$ methanolysis and ethylene glycolysis reactions, respectively. Using the slope of these graphs, the Ea values obtained for the $NaBH_4$ methanolysis and ethylene glycolysis reactions were found to be 37.29 kJ mol^{-1} and 50.00 kJ mol^{-1}, respectively. These values represent quite ideal values when compared to other catalysts reported in Table 2. The HGR and Ea values obtained for the H_2 release in methanol and ethylene glycol from $NaBH_4$ with different catalyst systems are given in Table 2 [17,20,45, 69–86].

In the literature, the Ea of the reaction of $NaBH_4$ (1 g) with methanol between 5 and 55 °C was found to be 13 kJ mol^{-1} [79]. At the same time, in another study, the Ea of the reaction of $NaBH_4$ (0.04 g) with methanol (18 ml) between − 20 and 50 °C was found to be 52 kJ mol^{-1} [78]. In the study, the Ea of the reaction of $NaBH_4$ (0.125 g) with methanol (10 ml) between 15 and 50 °C was found to be 43 kJ mol^{-1}.

For chitosan-zeolite-H-catalysed $NaBH_4$ methanolysis and ethylene glycolysis reactions, long-term reusability experiments were performed. For this purpose, 0.125 g of $NaBH_4$ at 30 °C, 10 ml of methanol or ethylene glycol, and 10 mg of catalyst were used. Five experiments were carried out in succession. After each experiment, the experiments were carried out by adding 0.125 g of $NaBH_4$ to the reaction vessel at the end of the H_2 production. The results obtained for the $NaBH_4$ methanolysis and ethylene glycolysis reactions are shown in Fig. 15a and 15b, respectively. 100% complete conversion was achieved in both reactions. However, a decrease in catalytic activity was observed at the end of each experiment. In the $NaBH_4$ methanolysis reaction, an HGR of 6666 ml $min^{-1}g^{-1}$ is obtained in the first cycle, but this HGR value decreases to 3000 ml $min^{-1}g^{-1}$ in the fifth cycle. Likewise, for the

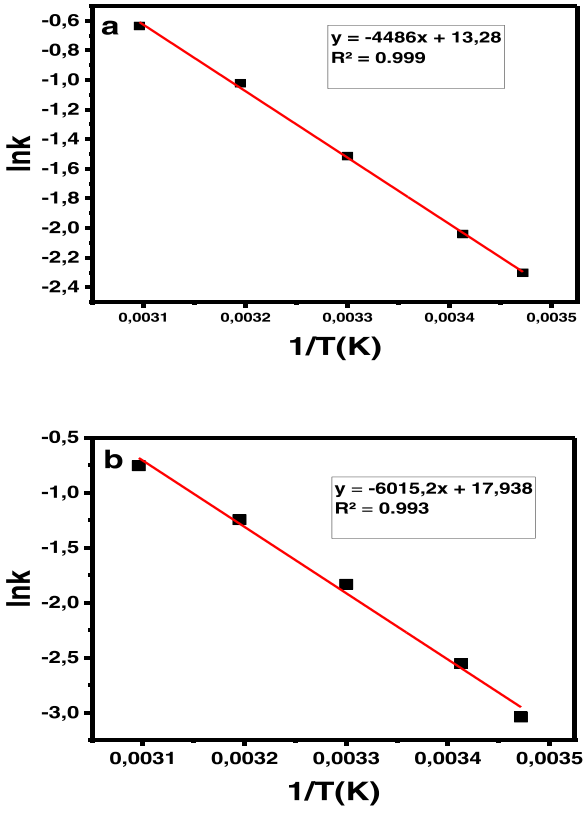

Fig. 14. Arrhenius plots obtained at different temperatures for the $NaBH_4$ methanolysis(a) and ethylene glycolysis(b) reactions,.

Table 2
Comparison of The HGR and Ea values obtained for the H_2 release in methanol and ethylene glycol from $NaBH_4$ with different catalyst systems.

Catalyst	HGR (ml min^{-1} g_{cat}^{-1})	Solvent	Ea (kJ·mol^{-1})	Reference
Methanol/no catalyst		methanol	13	[79]
Methanol/no catalyst		methanol	52	[78]
Methanol/no catalyst		methanol	43	This study
C-KOH-S-P	13,000	methanol	25.02	[80]
N-AC-N	16,250	methanol	11.45	[81]
CMS-$ZnCl_2$-Cu-B	4730	methanol	22.71	[82]
MWCNT-COOHs	8766	methanol	20.1	[86]
Poly(acrylic acid)/ polysaccharide IPN	8182	methanol	34.8	[69]
g-C_3N_4-TiO_2-P	14,750	methanol	36.17	[70]
g- C_3N_4-SiO_2-N	11,400	methanol	33.2	[71]
PEI-HFPA	3463	methanol	28.1	[72]
g– C_3N_4–EDTA-H	7571	methanol	35.6	[45]
Cu–Co/CH	1370	methanol		[73]
O doped g- C_3N_4	10,800	methanol	36.13	[20]
O doped AKOH + N	14,444	methanol	7.86	[74]
P doped PPCD	13,000	methanol	30.96	[75]
p (MTMA)	4838	methanol	24.1	[76]
S-AC-S-N	26,000	methanol	10.59	[83]
S-AC-N	10,105	methanol	39.75	[84]
p (AMPS)-TDA-1 PIL microgels	854	methanol	14.3	[77]
C–KOH–N	20,100	methanol	30.23	[85]
$NaBH_4$ ethylene glycolysis with 1 M H_3PO_4 catalysts	5800	ethylene glycol	24.45	[17]
$NaBH_4$ ethylene glycolysis with 1 M CH_3COOH	4542	ethylene glycol	33.23	[17]
Chitosan-zeolite-H	17,500	methanol	37.29	This study
Chitosan-zeolite-H	10,428	ethylene glycol	50.00	This study

$NaBH_4$ ethylene glycolysis reaction, an HGR value of 5666 ml $min^{-1}g^{-1}$ was obtained in the first cycle versus 3200 ml $min^{-1}g^{-1}$ in the fifth cycle. The possible reason for the decrease in catalytic activity for both reactions may be related to the inhibitory effect of the by-products between methanol and ethylene glycol on H_2 production by $NaBH_4$ on the chitosan-zeolite-H catalyst surface [87–89].

3.3. Possible mechanism of catalytic activities

Fig. 16 gives the H_2 volume from $NaBH_4$ methanolysis+chitosan-zeolite-H and ethylene glycolysis+chitosan-zeolite-H, only methanol+$NaBH_4$ and only ethylene glycol+$NaBH_4$ reactions. While this methanolysis reaction took about 15 min to complete with 0.125 g $NaBH_4$ in methanol only, it took about 17 min to complete this ethylene glycolysis reaction with 0.125 g $NaBH_4$ only in ethylene glycol medium. As can be understood, the H_2 production reaction took place in a shorter time in the methanol environment compared to the ethylene glycol environment.

The following steps for the methanolysis reaction can be written.

$$NaBH_4 \leftrightarrow Na^+ + BH_4^- \quad (4)$$

$$BH_4^- + H^+ \leftrightarrow BH_3 + H_2 \quad (5)$$

$$BH_3 + 3CH_3OH \rightarrow B(CH_3O)_3 + 3H_2 \quad (6)$$

$$B(CH_3O)_3 + CH_3OH \leftrightarrow B(CH_3O)_4^- + H^+ \quad (7)$$

$$4B(CH_3O)_4^- + 2H^+ + 7H_2O \leftrightarrow B_4O_7^{2-} + 16CH_3OH \quad (8)$$

The following reactions can be written for the mechanism of the

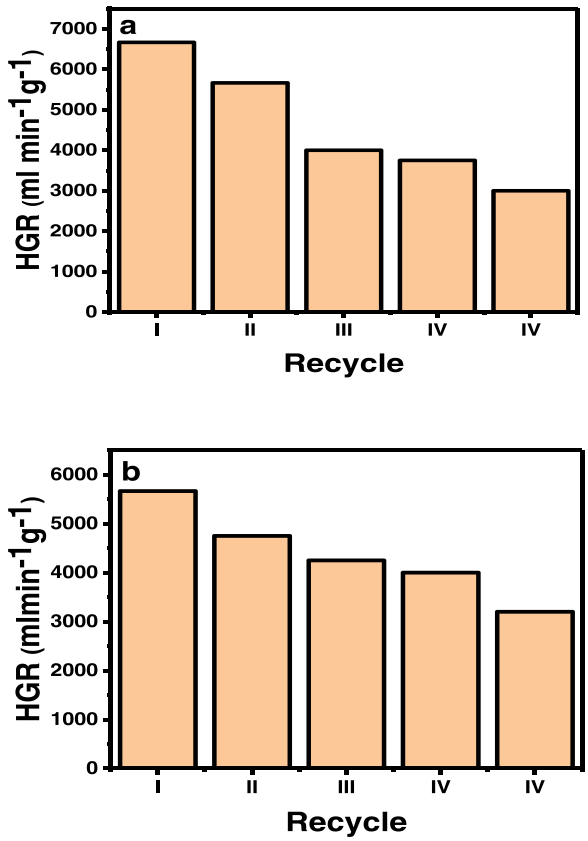

Fig. 15. Reusability experiments for the $NaBH_4$ methanolysis(a) and ethylene glycolysis(b) reactions.

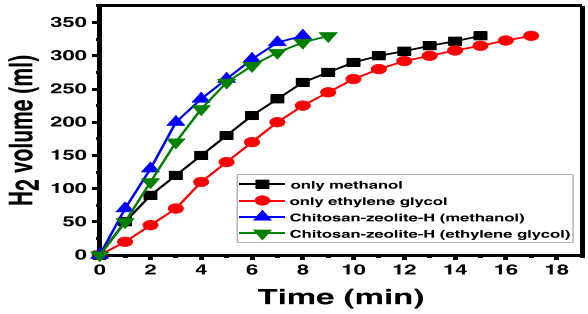

Fig. 16. H_2 volume from $NaBH_4$ methanolysis+chitosan-zeolite-H and ethylene glycolysis+chitosan-zeolite-H, only methanol+$NaBH_4$ and only ethylene glycol+$NaBH_4$ reactions.

$NaBH_4$ ethylene glycolysis reaction.

$$NaBH_4 \leftrightarrow Na^+ + BH_4^- \quad (9)$$

$$BH_4^- + H^+ \leftrightarrow BH_3 + H_2 \quad (10)$$

$$2BH_3 + 3C_2H_4(OH)_2 \rightarrow 2B(CH_2O)_3 + 6H_2 \quad (11)$$

$$2B(CH_2O)_3 + C_2H_4(OH)_2 \leftrightarrow 2B(CH_2O)_4^- + 2H^+ \quad (12)$$

$$4B(CH_2O)_4^- + 2H^+ + 7H_2O \leftrightarrow B_4O_7^{2-} + 8C_2H_4(OH)_2 \quad (13)$$

As can be understood from both methanol and ethylene glycol reactions, there is a faster H_2 production with increasing H^+ in the reaction medium. The possible reason for this result can be explained by the fact that methanol, which has a more acidic character at the beginning of the reaction compared to ethylene glycol, immediately reacts with $NaBH_4$ and produces H_2 faster on the catalyst surface. Normally, the pKa values for ethylene glycol and methanol at 25 °C are 14.22 and 15.2. These values indicate that ethylene glycol is more acidic than methanol. Therefore, according to Eq. (5) and Eq. (10), more efficient H_2 production can be expected in an ethylene glycol medium. However, ethylene glycol has a higher viscosity than methanol. The viscosity values of ethylene glycol and methanol at 300 K are 16.2 cP and 0.56 cP, respectively. Methanol has one -OH group per molecule while ethylene glycol has two -OH groups. Therefore, the viscosity, which depends on the amount of hydrogen bonding between the molecules, will increase due to the increase of the -OH bond in the molecule. Thus, ethylene glycol is more viscous than methanol. As the viscosity increases, the mobility of the particles in the solution slows down. Thus, slower reaction kinetics are involved. As can be seen in Fig. 16, H_2 production in methanol was more efficient in both catalyst and non-catalyst environments.

The methanol or ethylene glycol reacts with the sodium ion of $NaBH_4$ to form alkoxide. These reactions of alcohols can be an indication of their acidic nature. The acidic structure resulting from the proton in the hydroxyl groups of alcohols weakens due to the increase in the electron density of the oxygen atom by adding an electron-donating group to this hydroxyl group. Thus, it can be stated that methanol, which is less branched, has a more acidic structure compared to ethylene glycol. As can be seen in Eq. (5) and Eq. (10), the increase of H^+ ions in the solution environment positively supports the formation of H_2. Thus, as can be seen in Fig. 14, faster H_2 production was achieved with the methanol solvent compared to the ethylene glycol solvent.

Compatibility between the surfaces of materials used in hybrid catalyst systems is an important issue for catalytic performance.

In this study, both chitosan, a polymeric substance, and zeolite were used. As stated earlier, both materials were heat activated for an effective composite formation. Then, protonation with hydrochloric acid was performed to modify the surface of the composite hybrid material obtained. XRD, SEM-EDS, TEM, XPS and FTIR analyses showed a composite formation between chitosan and zeolite. Due to the deterioration of the structure of the zeolite as a result of the decrease in particle size, the collapse of the voids and a decrease in the specific surface area are in question. Table 1 confirms that the surface area of the zeolite is reduced. Therefore, the surface active sites and surface acidity of the chitosan-zeolite-H catalyst become important in the catalytic performance. The acid domains of the zeolite can reduce the activation energy of chain breaking and accelerate the free radical reaction. There is a similar approach in the literature [50]. The catalytic performance was significantly affected by the chitosan-zeolite-H catalyst obtained after protonation. Positively charged active sites were formed by protonation on the chitosan-zeolite-H surface obtained in this study. When zeolite is blended with chitosan, hydrogen bonds or acid-base ionic interactions are likely to form with SiO_2 in the zeolite structure and –OH and $–NH_2$ groups in the chitosan structure. Thus, a more compatible interface for the catalytic reaction is in question. XPS and FTIR analyses also supported the formation of hydrogen bonds on the chitosan/zeolite surface due to both interactions with hydrochloric acid and hybrid composite formation. In the hydrochloric acid medium, the zeolite is negatively charged, while the chitosan is positively charged, which combines with a polar interaction. Chitosan can be on either side of the zeolite. This provides the possibility of combining positively charged ions (H^+ or Na^+) with this negatively charged compound site through electrostatic interaction. In addition, a coordination bond can be formed between the positive ions and the –OH and $–NH_2$ groups in the composite.

Methoxide ions, which are formed when alcohol reacts with an OH^- ion, are highly nucleophilic molecules. Due to its nucleophilicity, methoxide can attack the carbonyl group of chitosan in the chitosan-zeolite structure. The nitrogen-containing electron pair in the amino groups of chitosan and the OH hydroxyl groups of chitosan also participate in the reaction [49,90]. On the other hand, after the interaction with hydrochloric acid, the $–NH_2$ groups of chitosan are

converted to NH_3^+ and the BH_4^- and CH_3O^- ions in the solution are easily adsorbed on the surface of this hybrid catalyst, positively promoting the formation of H_2.

As in clays, the basic components of zeolites are SiO_2 and Al_2O_3 layers. With acid treatment, protons penetrate mineral layers and react with structural OH groups. As a result of the resulting dehydroxylation, there is a sequential release of central atoms from the octahedral, as well as the removal of Al from the tetrahedral layers. Depending on the degree of acid activation, there is the formation of structurally unchanged layers and amorphous silica [91]. Decreased crystallinity can be confirmed in the XRD pattern. Chen et al. stated that the formation of more channels and acid regions in the catalyst structure in the clay structure modified with hydrochloric acid affects the catalytic activity [92]. It can be seen from the TEM images and XRD patterns that the particle sizes decrease after the interaction of the chitosan-zeolite sample with hydrochloric acid. In the catalytic process, the catalytic activity is positively affected as a result of the decrease in particle size [93]. Also, zeolites can be considered as Lewis acids and Lewis bases for adsorption processes due to their electron-donating and electron-accepting properties [49]. Therefore, positively charged functional groups or Lewis acids on the surface can interact via electrostatic interaction for negatively charged or basic species in solution, improving the catalytic activity of this methanolysis or ethylene glycolysis reactions. Thus, the active sites on catalyst systems are important for catalytic performance. It is reasonable to obtain higher catalytic performance with more protonated sites with the presence of more amine groups in the reaction of $NaBH_4$ methanolysis as an acid-catalysed reaction. Recently, in $NaBH_4$ methanolysis, there are alternative catalysts obtained from both the modification of cellulose-based materials with chitosan-like structures with amine group-containing agents and the HCl protonation process [19,61,94]. Again, similarly, Şahiner et al. proposed the Michaelis-Menten mechanism for the methanolysis of $NaBH_4$ catalysed by natural sands [95], amine-modified TiO_2 [96].

According to the Langmuir-Hinshelwood mechanism, both $NaBH_4$ and methanol molecules react on the catalyst surface [96,97]. However, functional groups containing a positive charge can increase the catalytic activity in these methanolysis and ethylene glycolysis reactions according to the Michaelis-Menten type mechanism. According to the Michaelis-Menten model, there is an interaction between the borohydride ion adsorbed on the catalyst surface and methanol or ethylene glycol, which is not adsorbed on the catalyst surface [97]. The positively charged chitosan-zeolite-H and borate anion react to form a complex. This complex then reacts with methanol or ethylene glycol to form H_2 and BH_3 to form a $CH_3O\text{-}BH_2$ or $CH_2OHCH_2O\text{-}BH_2$ molecule. After forming $B(OCH_3)_3$ with methanol and $2B(CH_2O)_3$ with ethylene glycol, H_2 is released. As a result, 4 equivalents of H_2 are obtained by reacting BH_4^- and protons of methanol or ethylene glycol. The positively charged species on the chitosan-zeolite-H hybrid composite surface affect the formation of H_2 more effectively by promoting the adsorption of methanol or ethylene glycol alkoxide and BH_4^- ions on the catalyst surface.

Fig. 17 shows the EDS analysis(a), FTIR analysis(b), XRD analysis(c), and SEM analysis (d, e) of the catalyst obtained after $NaBH_4$ methanolysis and $NaBH_4$ ethylene glycolysis reactions. According to Eqs. (1) and (2), $NaB(OCH_3)_4$ by-product is formed from the interaction between $NaBH_4$ and methanol, and $NaB(OCH_2)_4$ by-product is formed from the interaction between $NaBH_4$ and ethylene glycol. EDS analysis (a) of the catalyst obtained after $NaBH_4$ methanolysis and $NaBH_4$ ethylene glycolysis reactions confirms the presence of both sodium and boron atoms on the catalyst surface. FTIR analysis (b) of the related catalyst obtained after $NaBH_4$ methanolysis and $NaBH_4$ ethylene glycolysis reactions shows that there are significant changes, especially in the range of 500–1750 cm^{-1}. This result shows that especially functional groups in this range are effective in $NaBH_4$ methanolysis and $NaBH_4$ ethylene glycolysis reactions. This result shows that both positively charged groups such as NH_3^+ in the chitosan structure and oxygenated groups in the zeolite structure are effective, as stated before. Also, as can be seen in the FTIR spectrum, the peak intensities were significantly reduced in the spectrum obtained for the $NaBH_4$ methanolysis reaction compared to the $NaBH_4$ ethylene glycolysis reaction. This result suggests that H_2 production from the $NaBH_4$ methanolysis reaction with the related catalyst is more efficient than the $NaBH_4$ ethylene glycolysis reaction due to the

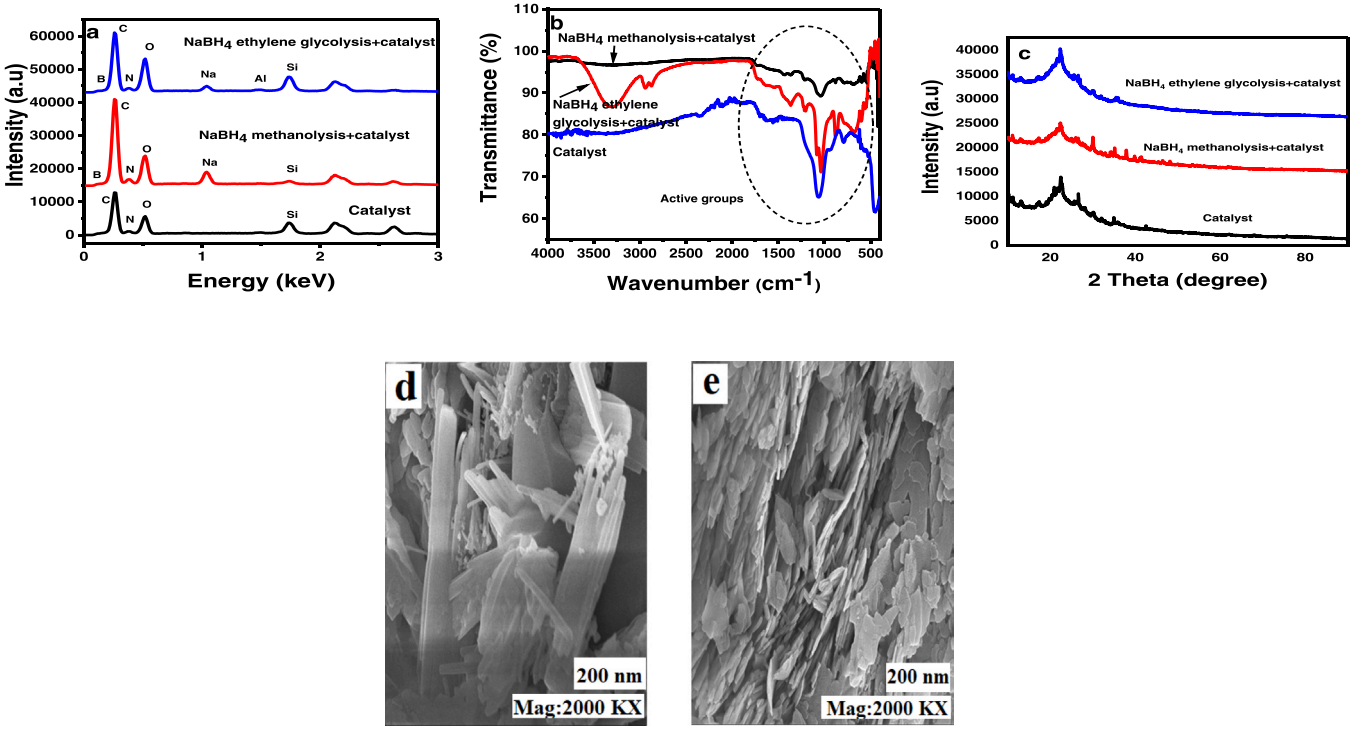

Fig. 17. EDS analysis(a), FTIR analysis(b), XRD analysis(c), SEM analysis (d, e) of the catalyst obtained after $NaBH_4$ methanolysis and $NaBH_4$ ethylene glycolysis reactions.

inclusion of active groups on the catalyst surface. The HGR values given in Table 2 also support this result. At the same time, XRD pattern(c) results obtained for the related catalyst after $NaBH_4$ methanolysis and $NaBH_4$ ethylene glycolysis reactions also support this conclusion. SEM images obtained after $NaBH_4$ methanolysis(d) and $NaBH_4$ ethylene glycolysis(e) reactions also show that the surface of the relevant catalyst becomes more heterogeneous and rough due to reactions.

The synthesis of chitosan-zeolite-H catalyst and possible H_2 production in methanol or ethylene glycol are presented in Fig. 18.

4. Conclusion

In this study, the synthesis of protonated chitosan-zeolite hybrid metal-free catalysts for efficient H_2 production from $NaBH_4$ methanolysis and $NaBH_4$ ethylene glycolysis reactions. HGR values of $NaBH_4$ (0.25 g) methanolysis and $NaBH_4$ (0.25 g) ethylene glycolysis were 17,500 and 10,414 ml $min^{-1}g^{-1}$, respectively. Ea values obtained for the $NaBH_4$ methanolysis and ethylene glycolysis reactions were found to be 37.29 kJ mol^{-1} and 50.00 kJ mol^{-1}, respectively. The prepared chitosan/zeolite-H composite was characterized by XRD, SEM-EDS, FTIR, TEM and XPS analyses. The XRD diffraction diagram of the chitosan-zeolite-H shows the successful formation of the composite compound. The SEM image of the chitosan-zeolite-H composite shows that both the chitosan becomes more porous with hydrochloric acid and the zeolite is uniformly dispersed in the chitosan matrix with a layered structure. The TEM image of the chitosan-zeolite-H composite shows that the zeolite is homogeneously dispersed in the chitosan matrix. The presence of C, O N and Si atoms as the main components of the chitosan-zeolite-H composite XPS and EDS analyses shows that the chitosan and zeolite composite composition was formed successfully. FTIR spectrum for chitosan-zeolite-H demonstrates the successful integration between chitosan and zeolite. Also, the possible mechanism of H_2 formation in methanol and ethylene glycol with chitosan-zeolite-H is discussed. XPS and FTIR analyses also supported the formation of hydrogen bonds on the chitosan-zeolite surface due to both interactions with hydrochloric acid and hybrid composite formation. The catalytic performance was significantly affected by the chitosan-zeolite-H catalyst obtained after protonation. EDS analysis of the catalyst obtained after $NaBH_4$ methanolysis and $NaBH_4$ ethylene glycolysis reactions confirms the presence of both sodium and boron atoms on the catalyst surface. FTIR analysis of the catalyst obtained after $NaBH_4$ methanolysis and $NaBH_4$ ethylene glycolysis reactions shows that there are significant changes, especially in the range of 500–1750 cm^{-1}. This result shows that especially functional groups in this range are effective in $NaBH_4$ methanolysis and $NaBH_4$ ethylene glycolysis reactions.

CRediT authorship contribution statement

Cafer SAKA: Conceptualization, Methodology, Software Writing – original draft preparation. Investigation, Writing – review & editing,

Declaration of Competing Interest

The authors declare that they have no known competing financialinterestsor personal relationships that could have appeared to influence the work reported in this paper.

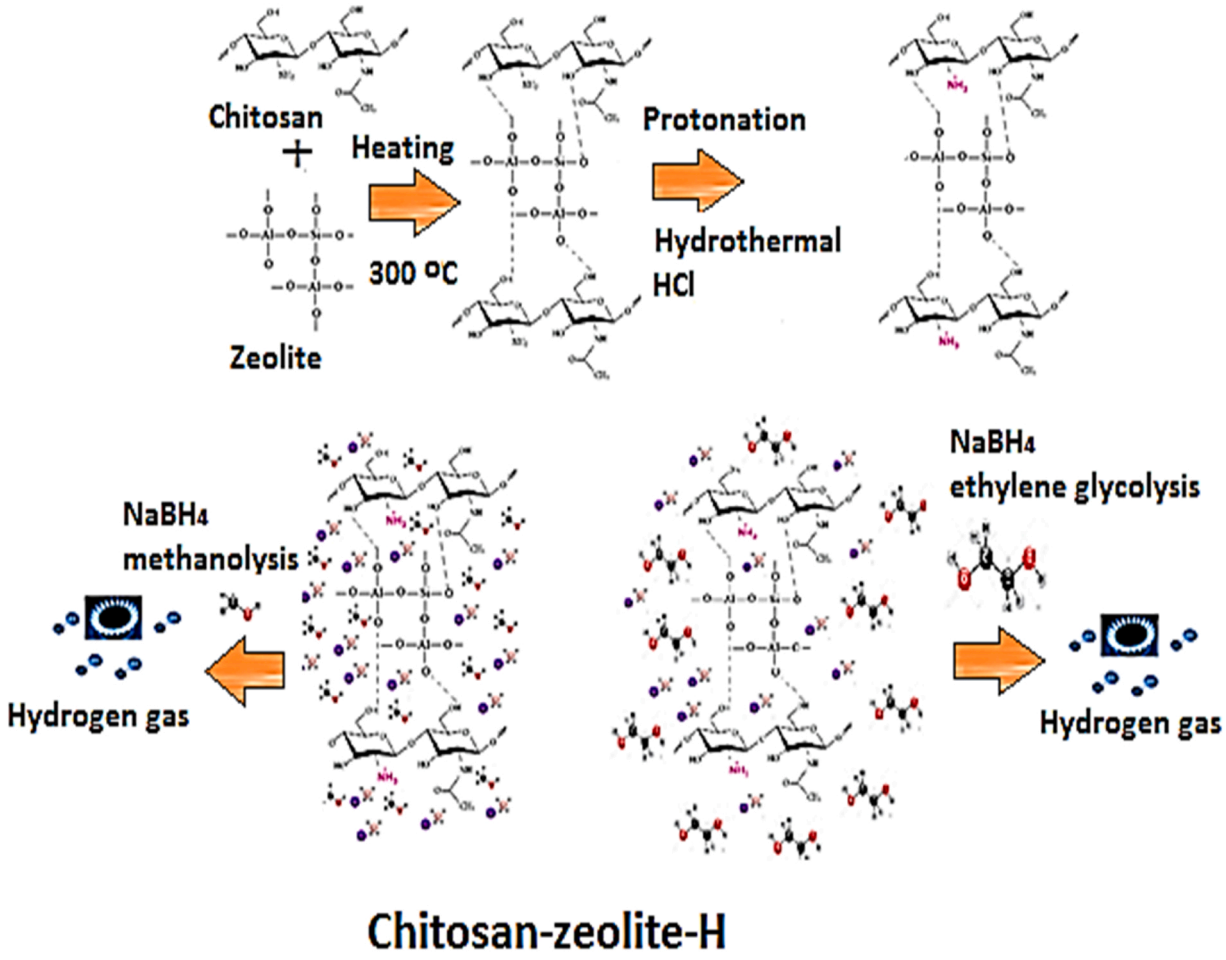

Fig. 18. The synthesis of chitosan-zeolite-H catalyst and possible H_2 production in methanol or ethylene glycol.

Data Availability

No data was used for the research described in the article.

References

[1] J. Ji, K. Deng, J. Li, Z. Zhang, X. Duan, H. Huang, In situ transformation of 3D Co_3O_4 nanoparticles to 2D nanosheets with rich surface oxygen vacancies to boost hydrogen generation from $NaBH_4$, Chem. Eng. J. 424 (2021), https://doi.org/10.1016/J.CEJ.2021.130350.

[2] N. Selvitepe, A. Balbay, C. Saka, Optimisation of sepiolite clay with phosphoric acid treatment as support material for CoB catalyst and application to produce hydrogen from the $NaBH_4$ hydrolysis, Int. J. Hydrog. Energy (2019), https://doi.org/10.1016/j.ijhydene.2019.04.254.

[3] C. Saka, A. Balbay, Influence of process parameters on enhanced hydrogen evolution from alcoholysis of sodium borohydride with a boric acid catalyst, Int. J. Hydrog. Energy 45 (2020) 16193–16200, https://doi.org/10.1016/j.ijhydene.2020.04.094.

[4] K.N. Patil, D. Prasad, Bhagyashree, V.K. Manoorkar, W. Nabgan, B.M. Nagaraja, A. H. Jadhav, Engineered nano-foam of tri-metallic (FeCuCo) oxide catalyst for enhanced hydrogen generation via $NaBH_4$ hydrolysis, Chemosphere 281 (2021), 130988, https://doi.org/10.1016/J.CHEMOSPHERE.2021.130988.

[5] D. Prasad, K.N. Patil, N. Sandhya, C.R. Chaitra, J.T. Bhanushali, A.K. Samal, R. S. Keri, A.H. Jadhav, B.M. Nagaraja, Highly efficient hydrogen production by hydrolysis of NaBH4 using eminently competent recyclable Fe_2O_3 decorated oxidized MWCNTs robust catalyst, Appl. Surf. Sci. (2019), https://doi.org/10.1016/j.apsusc.2019.06.041.

[6] K.N. Patil, D. Prasad, J.T. Bhanushali, H. Kim, A.B. Atar, B.M. Nagaraja, A. H. Jadhav, Sustainable hydrogen generation by catalytic hydrolysis of $NaBH_4$ using tailored nanostructured urchin-like $CuCo_2O_4$ spinel catalyst, Catal. Lett. 150 (2020) 586–604, https://doi.org/10.1007/S10562-019-03025-W/TABLES/1.

[7] D. Prasad, K.N. Patil, C.R. Chaitra, N. Sandhya, J.T. Bhanushali, S.W. Gosavi, A. H. Jadhav, B.M. Nagaraja, Sulfonic acid functionalized PVA/PVDF composite hollow microcapsules: Highly phenomenal & recyclable catalysts for sustainable hydrogen production, Appl. Surf. Sci. 488 (2019) 714–727, https://doi.org/10.1016/J.APSUSC.2019.05.193.

[8] N. Sahiner, A.O. Yasar, N. Aktas, Metal-free pyridinium-based polymeric ionic liquids as catalyst for H_2 generation from $NaBH_4$, Renew. Energy (2017), https://doi.org/10.1016/j.renene.2016.09.066.

[9] A.A. Kassem, H.N. Abdelhamid, D.M. Fouad, S.A. Ibrahim, Metal-organic frameworks (MOFs) and MOFs-derived CuO@C for hydrogen generation from sodium borohydride, Int. J. Hydrog. Energy (2019), https://doi.org/10.1016/j.ijhydene.2019.10.047.

[10] S.B. Khan, Metal nanoparticles containing chitosan wrapped cellulose nanocomposites for catalytic hydrogen production and reduction of environmental pollutants, Carbohydr. Polym. (2020), https://doi.org/10.1016/j.carbpol.2020.116286.

[11] C. Saka, A. Balbay, Fast and effective hydrogen production from ethanolysis and hydrolysis reactions of potassium borohydride using phosphoric acid, Int. J. Hydrog. Energy 43 (2018) 19976–19983, https://doi.org/10.1016/j.ijhydene.2018.09.048.

[12] G.M. Arzac, A. Fernández, Hydrogen production through sodium borohydride ethanolysis, Int. J. Hydrog. Energy 40 (2015) 5326–5332, https://doi.org/10.1016/j.ijhydene.2015.01.115.

[13] D.-W. Zhuang, H.-B. Dai, P. Wang, Hydrogen generation from solvolysis of sodium borohydride in ethylene glycol–water mixtures over a wide range of temperature, RSC Adv. 3 (2013) 23810–23815, https://doi.org/10.1039/C3RA43136C.

[14] H. Ould-Amara, D. Alligier, E. Petit, P.G. Yot, U.B. Demirci, Sodium borohydride and propylene glycol, an effective combination for the generation of 2.3 wt% of hydrogen, Int. J. Hydrog. Energy (2018), https://doi.org/10.1016/j.ijhydene.2018.02.169.

[15] E. Fiedler, G. Grossmann, D.B. Kersebohm, G. Weiss, C. Witte, Methanol, in: Ullmann's Encyclopedia of Industrial Chemistry, Wiley-VCH Verlag GmbH & Co. KGaA, Weinheim, Germany, 2000, pp. 635–645, https://doi.org/10.1002/14356007.a16_465.

[16] B.Y. Yu, I.L. Chien, Design and optimization of dimethyl oxalate (DMO) hydrogenation process to produce ethylene glycol (EG), Chem. Eng. Res. Des. 121 (2017) 173–190, https://doi.org/10.1016/J.CHERD.2017.03.012.

[17] C. Saka, A. Balbay, Ethylene glycol as an alternative solvent approach for very efficient hydrogen production from sodium borohydride with phosphoric acid and acetic acid catalysts, Int. J. Hydrog. Energy 47 (2022) 10500–10507, https://doi.org/10.1016/J.IJHYDENE.2022.01.131.

[18] M.W. Abebe, A.F. Baye, H. Kim, Poly (acrylic acid)/polysaccharides IPN derived metal free catalyst for rapid hydrogen generation via $NaBH_4$ methanolysis, Int. J. Hydrog. Energy 47 (2022) 32060–32070, https://doi.org/10.1016/J.IJHYDENE.2022.07.106.

[19] F. Ali, S.B. Khan, A.M. Asiri, Chitosan coated cellulose cotton fibers as catalyst for the H_2 production from $NaBH_4$ methanolysis, Int. J. Hydrog. Energy 44 (2019) 4143–4155, https://doi.org/10.1016/J.IJHYDENE.2018.12.158.

[20] C. Saka, Surface modification with oxygen doping of g-C_3N_4 nanoparticles by carbon vacancy for efficient dehydrogenation of sodium borohydride in methanol, Fuel 310 (2022), 122444, https://doi.org/10.1016/J.FUEL.2021.122444.

[21] C. Saka, Highly active and durable hydrogen release in $NaBH_4$ methanolysis reaction with sulphur and phosphorus-doped metal-free microalgal carbon nanoparticles, Appl. Catal. B Environ. 292 (2021), 120165, https://doi.org/10.1016/j.apcatb.2021.120165.

[22] E. Meşe, A. Kantürk Figen, B. Coşkuner Filiz, S. Pişkin, Cobalt-boron loaded thermal activated Turkish sepiolite composites (Co-B@tSe) as a catalyst for hydrogen delivery, Appl. Clay Sci. (2018), https://doi.org/10.1016/j.clay.2017.12.008.

[23] P. Dai, Y. Yao, E. Hu, D. Xu, Z. Li, C. Wang, Self-assembled ZIF-67@graphene oxide as a cobalt-based catalyst precursor with enhanced catalytic activity toward methanolysis of sodium borohydride, Appl. Surf. Sci. 546 (2021), 149128, https://doi.org/10.1016/j.apsusc.2021.149128.

[24] M. Dohendou, K. Pakzad, Z. Nezafat, M. Nasrollahzadeh, M.G. Dekamin, Progresses in chitin, chitosan, starch, cellulose, pectin, alginate, gelatin and gum based (nano) catalysts for the Heck coupling reactions: a review, Int. J. Biol. Macromol. 192 (2021) 771–819, https://doi.org/10.1016/J.IJBIOMAC.2021.09.162.

[25] N.M. Mahmoodi, M. Oveisi, A. Taghizadeh, M. Taghizadeh, Synthesis of pearl necklace-like ZIF-8@chitosan/PVA nanofiber with synergistic effect for recycling aqueous dye removal, Carbohydr. Polym. 227 (2020), 115364, https://doi.org/10.1016/J.CARBPOL.2019.115364.

[26] A. Wang, J. Ni, W. Wang, D. Liu, Q. Zhu, B. Xue, C.C. Chang, J. Ma, Y. Zhao, MOF derived Co−Fe nitrogen doped graphite carbon@crosslinked magnetic chitosan Micro−nanoreactor for environmental applications: synergy enhancement effect of adsorption−PMS activation, Appl. Catal. B Environ. 319 (2022), 121926, https://doi.org/10.1016/J.APCATB.2022.121926.

[27] B. Chen, X. Zheng, J. Gu, S. Qiu, J. Song, X. Wu, H. Dong, Q. Zhang, T. Wang, Engineering Sn doping Ni/chitosan to boost higher alcohols synthesis from direct coupling of aqueous ethanol: Modifying adsorption of aldehyde intermediates for C-C bond cleavage suppressing, Appl. Catal. B Environ. 321 (2023), 122048, https://doi.org/10.1016/J.APCATB.2022.122048.

[28] Y. Li, J. Ma, D. Jin, G. Jiao, X. Yang, K. Liu, J. Zhou, R. Sun, Copper oxide functionalized chitosan hybrid hydrogels for highly efficient photocatalytic-reforming of biomass-based monosaccharides to lactic acid, Appl. Catal. B Environ. 291 (2021), 120123, https://doi.org/10.1016/J.APCATB.2021.120123.

[29] Y. Fu, L. Qin, D. Huang, G. Zeng, C. Lai, B. Li, J. He, H. Yi, M. Zhang, M. Cheng, X. Wen, Chitosan functionalized activated coke for Au nanoparticles anchoring: Green synthesis and catalytic activities in hydrogenation of nitrophenols and azo dyes, Appl. Catal. B Environ. 255 (2019), 117740, https://doi.org/10.1016/J.APCATB.2019.05.042.

[30] Á. Molnár, The use of chitosan-based metal catalysts in organic transformations, Coord. Chem. Rev. 388 (2019) 126–171, https://doi.org/10.1016/J.CCR.2019.02.018.

[31] W. Suginta, P. Khunkaewla, A. Schulte, Electrochemical biosensor applications of polysaccharides chitin and chitosan, Chem. Rev. 113 (2013) 5458–5479, https://doi.org/10.1021/CR300325R.

[32] D. Liang, Y. Wang, M. Chen, X. Xie, C. Li, J. Wang, L. Yuan, Dry reforming of methane for syngas production over attapulgite-derived MFI zeolite encapsulated bimetallic Ni-Co catalysts, Appl. Catal. B Environ. (2022), 122088, https://doi.org/10.1016/J.APCATB.2022.122088.

[33] L. Ge, M. Qiu, Y. Zhu, S. Yang, W. Li, W. Li, Z. Jiang, X. Chen, Synergistic catalysis of Ru single-atoms and zeolite boosts high-efficiency hydrogen storage, Appl. Catal. B Environ. 319 (2022), 121958, https://doi.org/10.1016/J.APCATB.2022.121958.

[34] A. Ates, Characteristics of Fe-exchanged natural zeolites for the decomposition of N_2O and its selective catalytic reduction with NH_3, Appl. Catal. B Environ. 76 (2007) 282–290, https://doi.org/10.1016/J.APCATB.2007.06.005.

[35] V. Van Speybroeck, K. Hemelsoet, L. Joos, M. Waroquier, R.G. Bell, C.R.A. Catlow, Advances in theory and their application within the field of zeolite chemistry, Chem. Soc. Rev. 44 (2015) 7044–7111, https://doi.org/10.1039/C5CS00029G.

[36] M. Choi, K. Na, J. Kim, Y. Sakamoto, O. Terasaki, R. Ryoo, Stable single-unit-cell nanosheets of zeolite MFI as active and long-lived catalysts, Nat 2009 4617261 461 (2009) 246–249, https://doi.org/10.1038/nature08288.

[37] B. Wang, X. Yan, X. Zhang, H. Zhang, F. Li, Citric acid-modified beta zeolite for polyoxymethylene dimethyl ethers synthesis: The textural and acidic properties regulation, Appl. Catal. B Environ. 266 (2020), 118645, https://doi.org/10.1016/J.APCATB.2020.118645.

[38] Z. Zhu, H. Ma, W. Liao, P. Tang, K. Yang, T. Su, W. Ren, H. Lü, Insight into tri-coordinated aluminum dependent catalytic properties of dealuminated Y zeolites in oxidative desulfurization, Appl. Catal. B Environ. 288 (2021), 120022, https://doi.org/10.1016/J.APCATB.2021.120022.

[39] Y. Xue, J. Li, P. Wang, X. Cui, H. Zheng, Y. Niu, M. Dong, Z. Qin, J. Wang, W. Fan, Regulating Al distribution of ZSM-5 by Sn incorporation for improving catalytic properties in methanol to olefins, Appl. Catal. B Environ. 280 (2021), 119391, https://doi.org/10.1016/J.APCATB.2020.119391.

[40] Y. Li, S. Huang, Z. Cheng, K. Cai, L. Li, E. Milan, J. Lv, Y. Wang, Q. Sun, X. Ma, Promoting the activity of Ce-incorporated MOR in dimethyl ether carbonylation through tailoring the distribution of Brønsted acids, Appl. Catal. B Environ. 256 (2019), 117777, https://doi.org/10.1016/J.APCATB.2019.117777.

[41] M. Sajjadi, M. Nasrollahzadeh, H. Ghafuri, T. Baran, Y. Orooji, N.Y. Baran, M. Shokouhimehr, Modified chitosan-zeolite supported Pd nanoparticles: a reusable catalyst for the synthesis of 5-substituted-1H-tetrazoles from aryl halides, Int. J. Biol. Macromol. 209 (2022) 1573–1585, https://doi.org/10.1016/J.IJBIOMAC.2022.04.075.

[42] Y. Zhang, W. Yan, Z. Sun, C. Pan, X. Mi, G. Zhao, J. Gao, Fabrication of porous zeolite/chitosan monoliths and their applications for drug release and metal ions adsorption, Carbohydr. Polym. 117 (2015) 657–665, https://doi.org/10.1016/J.CARBPOL.2014.09.018.

[43] G. Mahmodi, P. Zarrintaj, A. Taghizadeh, M. Taghizadeh, S. Manouchehri, S. Dangwal, A. Ronte, M.R. Ganjali, J.D. Ramsey, S.J. Kim, M.R. Saeb, From

microporous to mesoporous mineral frameworks: an alliance between zeolite and chitosan, Carbohydr. Res. 489 (2020), 107930, https://doi.org/10.1016/J.CARRES.2020.107930.
[44] M. Vakili, A. Mojiri, H.M. Zwain, J. Yuan, A.S. Giwa, W. Wang, F. Gholami, X. Guo, G. Cagnetta, G. Yu, Effect of beading parameters on cross-linked chitosan adsorptive properties, React. Funct. Polym. 144 (2019), 104354, https://doi.org/10.1016/J.REACTFUNCTPOLYM.2019.104354.
[45] C. Saka, Performance of g-C3N4 nanoparticles by EDTA modification and protonation for hydrogen release from sodium borohydride methanolysis, Int. J. Hydrog. Energy 47 (2022) 13654–13663, https://doi.org/10.1016/J.IJHYDENE.2022.02.121.
[46] J. Andrieux, U.B. Demirci, P. Miele, Langmuir–Hinshelwood kinetic model to capture the cobalt nanoparticles-catalyzed hydrolysis of sodium borohydride over a wide temperature range, Catal. Today 170 (2011) 13–19, https://doi.org/10.1016/J.CATTOD.2011.01.019.
[47] C. Saka, M. Salih Eygi, A. Balbay, CoB doped acid modified zeolite catalyst for enhanced hydrogen release from sodium borohydride hydrolysis, Int. J. Hydrog. Energy (2020), https://doi.org/10.1016/j.ijhydene.2020.03.238.
[48] Y. He, H. Lin, Y. Dong, B. Li, L. Wang, S. Chu, M. Luo, J. Liu, Zeolite supported Fe/Ni bimetallic nanoparticles for simultaneous removal of nitrate and phosphate: Synergistic effect and mechanism, Chem. Eng. J. (2018), https://doi.org/10.1016/j.cej.2018.04.088.
[49] L. Fereidooni, A. Abbaspourrad, M. Enayati, Electrolytic transesterification of waste frying oil using Na+/zeolite–chitosan biocomposite for biodiesel production, Waste Manag 127 (2021) 48–62, https://doi.org/10.1016/J.WASMAN.2021.04.020.
[50] W. Luo, Q. Hu, Z. yi Fan, J. Wan, Q. He, S. Xiong Huang, N. Zhou, M. Song, J. Chao Zhang, Z. Zhou, The effect of different particle sizes and HCl-modified kaolin on catalytic pyrolysis characteristics of reworked polypropylene plastics, Energy 213 (2020), 119080, https://doi.org/10.1016/J.ENERGY.2020.119080.
[51] M.M. Chambi-Peralta, A.C. Vieira Coelho, F. Machado de Souza Carvalho, S. M. Toffoli, Effects of exchanged cation, acid treatment and high shear mechanical treatment on the swelling and the particle size distribution of vermiculite, Appl. Clay Sci. 155 (2018) 1–7, https://doi.org/10.1016/J.CLAY.2017.12.049.
[52] Y. Lu, H. Zhang, Q. Wang, A. Wang, Hydrochloric acid pretreatment combined with microwave-assisted oxalic acid leaching of natural red palygorskite-rich clay for efficiently change the color and properties, Appl. Clay Sci. 228 (2022), 106594, https://doi.org/10.1016/J.CLAY.2022.106594.
[53] I. Corazzari, R. Nisticò, F. Turci, M.G. Faga, F. Franzoso, S. Tabasso, G. Magnacca, Advanced physico-chemical characterization of chitosan by means of TGA coupled on-line with FTIR and GCMS: thermal degradation and water adsorption capacity, Polym. Degrad. Stab. 112 (2015) 1–9, https://doi.org/10.1016/J.POLYMDEGRADSTAB.2014.12.006.
[54] J.A. Arcibar-Orozco, A.I. Flores-Rojas, J.R. Rangel-Mendez, P.E. Díaz-Flores, Synergistic effect of zeolite/chitosan in the removal of fluoride from aqueous solution 41 (2018) 1554–1567, https://doi.org/10.1080/09593330.2018.1542033. ⟨Https://Doi.Org/10.1080/09593330.2018.1542033⟩.
[55] W. Mozgawa, M. Sitarz, M. Rokita, Spectroscopic studies of different aluminosilicate structures, J. Mol. Struct. 511–512 (1999) 251–257, https://doi.org/10.1016/S0022-2860(99)00165-9.
[56] K.L.M. Taaca, M.R. Vasquez, Fabrication of Ag-exchanged zeolite/chitosan composites and effects of plasma treatment, Microporous Mesoporous Mater. 241 (2017) 383–391, https://doi.org/10.1016/J.MICROMESO.2017.01.002.
[57] S. Kumar, R. Bera, N. Das, J. Koh, Chitosan-based zeolite-Y and ZSM-5 porous biocomposites for H_2 and CO_2 storage, Carbohydr. Polym. 232 (2020), 115808, https://doi.org/10.1016/J.CARBPOL.2019.115808.
[58] X. Liu, Y. Zhang, Y. Liu, T. Zhang, Green method to synthesize magnetic zeolite/chitosan composites and adsorption of hexavalent chromium from aqueous solutions, Int. J. Biol. Macromol. 194 (2022) 746–754, https://doi.org/10.1016/J.IJBIOMAC.2021.11.121.
[59] L. Yu, J. Gong, C. Zeng, L. Zhang, Preparation of zeolite-A/chitosan hybrid composites and their bioactivities and antimicrobial activities, Mater. Sci. Eng. C. 33 (2013) 3652–3660, https://doi.org/10.1016/J.MSEC.2013.04.055.
[60] D. Yang, J. Li, Z. Jiang, L. Lu, X. Chen, Chitosan/TiO_2 nanocomposite pervaporation membranes for ethanol dehydration, Chem. Eng. Sci. 64 (2009) 3130–3137, https://doi.org/10.1016/J.CES.2009.03.042.
[61] N. Sahiner, S. Demirci, Natural microgranular cellulose as alternative catalyst to metal nanoparticles for H_2 production from $NaBH_4$ methanolysis, Appl. Catal. B Environ. 202 (2017) 199–206, https://doi.org/10.1016/j.apcatb.2016.09.028.
[62] Y. Dong, J. Bi, S. Ming, S. Zhang, D. Zhu, D. Meng, T. Li, Functionalized chitosan as a novel support for stabilizing palladium in Suzuki reactions, Carbohydr. Polym. 260 (2021), 117815, https://doi.org/10.1016/J.CARBPOL.2021.117815.
[63] A. Balakrishnan, S. Appunni, K. Gopalram, Immobilized TiO_2/chitosan beads for photocatalytic degradation of 2,4-dichlorophenoxyacetic acid, Int. J. Biol. Macromol. 161 (2020) 282–291, https://doi.org/10.1016/J.IJBIOMAC.2020.05.204.
[64] Z. Yu, X. Zhang, Y. Huang, Magnetic chitosan-iron(III) hydrogel as a fast and reusable adsorbent for chromium(VI) removal, Ind. Eng. Chem. Res. 52 (2013) 11956–11966, https://doi.org/10.1021/IE400781N/SUPPL_FILE/IE400781N_SI_001.PDF.
[65] M. Hong, L. Zhang, H. Fang, X. Feng, Z. Li, Surface engineering of CdS quantum dots modified SiO2@C3N4 nanospheres for effective photocatalytic hydrogen evolution, Mater. Sci. Semicond. Process. 136 (2021), 106134, https://doi.org/10.1016/J.MSSP.2021.106134.
[66] I.S. Amiinu, Z. Pu, X. Liu, K.A. Owusu, H.G.R. Monestel, F.O. Boakye, H. Zhang, S. Mu, Multifunctional Mo–N/C@MoS_2 electrocatalysts for HER, OER, ORR, and Zn–air batteries, Adv. Funct. Mater. 27 (2017), https://doi.org/10.1002/adfm.201702300.
[67] O. Al-Fulaij, A.Z.A. Elassar, F. Alsagheer, Utility of newly modified chitosan in the removal of heavy metal ions from aqueous medium: ion selectivity, XPS and TGA, Bull. Mater. Sci. 42 (2019) 1–12, https://doi.org/10.1007/S12034-019-1925-Y/FIGURES/11.
[68] S. Ismadji, D.S. Tong, F.E. Soetaredjo, A. Ayucitra, W.H. Yu, C.H. Zhou, Bentonite hydrochar composite for removal of ammonium from Koi fish tank, Appl. Clay Sci. 119 (2016) 146–154, https://doi.org/10.1016/J.CLAY.2015.08.022.
[69] M.W. Abebe, A.F. Baye, H. Kim, Poly (acrylic acid)/polysaccharides IPN derived metal free catalyst for rapid hydrogen generation via $NaBH_4$ methanolysis, Int. J. Hydrog. Energy (2022), https://doi.org/10.1016/J.IJHYDENE.2022.07.106.
[70] C. Saka, Phosphorus decorated g-C_3N_4-TiO_2 particles as efficient metal-free catalysts for hydrogen release by $NaBH_4$ methanolysis, Fuel 322 (2022), 124196, https://doi.org/10.1016/J.FUEL.2022.124196.
[71] C. Saka, Efficient and durable H_2 production from $NaBH_4$ methanolysis using N doped hybrid g-C_3N_4-SiO_2 composites with ammonia as a nitrogen source, Fuel 324 (2022), 124594, https://doi.org/10.1016/J.FUEL.2022.124594.
[72] S. Demirci, S.S. Suner, M. Yildiz, N. Sahiner, Polymeric ionic liquid forms of PEI microgels as catalysts for hydrogen production via sodium borohydride methanolysis, J. Mol. Liq. 360 (2022), 119562, https://doi.org/10.1016/J.MOLLIQ.2022.119562.
[73] E.M. Bakhsh, M.S.J. Khan, K. Akhtar, S.B. Khan, A.M. Asiri, Chitosan hydrogel wrapped bimetallic nanoparticles based efficient catalysts for the catalytic removal of organic pollutants and hydrogen production, Appl. Organomet. Chem. 36 (2022), e6741, https://doi.org/10.1002/AOC.6741.
[74] C. Saka, A. Balbay, Metal-free catalyst fabrication by incorporating oxygen groups on the surface of the carbonaceous sample and efficient hydrogen production from $NaBH_4$ methanolysis, Int. J. Hydrog. Energy 47 (2022) 7242–7251, https://doi.org/10.1016/J.IJHYDENE.2021.12.070.
[75] S. Samatya Ölmez, A. Balbay, C. Saka, Phosphorus doped carbon nanodots particles based on pomegranate peels for highly active dehydrogenation of sodium borohydride in methanol, Int. J. Hydrog. Energy (2022), https://doi.org/10.1016/J.IJHYDENE.2022.07.091.
[76] O.F. Ozturk, S. Demirci, S.B. Sengel, N. Sahiner, Highly regenerable ionic liquid microgels as inherently metal-free green catalyst for H2 generation, Polym. Adv. Technol. 29 (2018) 1426–1434, https://doi.org/10.1002/PAT.4254.
[77] S. Demirci, T. Zekoski, N. Sahiner, The preparation and use of p(2-acrylamido-2-methyl-1-propanesulfonic acid)-tris(dioxa-3,6-heptyl)amine (p(AMPS)-TDA-1) ionic liquid microgel in hydrogen production, Polym. Bull. 76 (2019) 1717–1735, https://doi.org/10.1007/S00289-018-2465-0.
[78] C.T.F. Lo, K. Karan, B.R. Davis, Kinetic studies of reaction between sodium borohydride and methanol, water, and their mixtures, Ind. Eng. Chem. Res. 46 (2007) 5478–5484, https://doi.org/10.1021/ie0608861.
[79] V.R. Fernandes, A.M.F.R. Pinto, C.M. Rangel, Hydrogen production from sodium borohydride in methanol-water mixtures, Int. J. Hydrog. Energy (2010), https://doi.org/10.1016/j.ijhydene.2009.11.064.
[80] C. Saka, Highly active and durable hydrogen release in $NaBH_4$ methanolysis reaction with sulphur and phosphorus-doped metal-free microalgal carbon nanoparticles, Appl. Catal. B Environ. 292 (2021), 120165, https://doi.org/10.1016/j.apcatb.2021.120165.
[81] C. Saka, A. Balbay, Oxygen and nitrogen-functionalized porous carbon particles derived from hazelnut shells for the efficient catalytic hydrogen production reaction, Biomass. Bioenergy 149 (2021), 106072, https://doi.org/10.1016/j.biombioe.2021.106072.
[82] C. Saka, M. Kaya, M. Bekiroğullari, Chlorella vulgaris microalgae strain modified with zinc chloride as a new support material for hydrogen production from $NaBH_4$ methanolysis using CuB, NiB, and FeB metal catalysts, Int. J. Hydrog. Energy 45 (2020) 1959–1968, https://doi.org/10.1016/j.ijhydene.2019.11.106.
[83] C. Saka, Sulphur and nitrogen-doped metal-free microalgal carbon catalysts for very active dehydrogenation of sodium borohydride in methanol, Int. J. Hydrog. Energy 46 (2021) 18326–18337, https://doi.org/10.1016/j.ijhydene.2021.03.001.
[84] C. Saka, Oxygen and nitrogen-doped metal-free microalgae carbon nanoparticles for efficient hydrogen production from sodium borohydride in methanol, Int. J. Hydrog. Energy 46 (2021) 26298–26307, https://doi.org/10.1016/j.ijhydene.2021.05.111.
[85] C. Saka, Very efficient dehydrogenation of methanolysis reaction with nitrogen doped Chlorella vulgaris microalgae carbon as metal-free catalysts, Int. J. Hydrog. Energy 46 (2021) 20961–20971, https://doi.org/10.1016/J.IJHYDENE.2021.03.220.
[86] N. Sahiner, Modified multi-wall carbon nanotubes as metal free catalyst for application in H_2 production from methanolysis of NaBH4, J. Power Sources 366 (2017) 178–184, https://doi.org/10.1016/j.jpowsour.2017.09.041.
[87] M.B. Swami, A.H. Jadhav, S.R. Mathpati, H.G. Ghuge, S.G. Patil, Eco-friendly highly efficient solvent free synthesis of benzimidazole derivatives over sulfonic acid functionalized graphene oxide in ambient condition, Res. Chem. Intermed. 43 (2017) 2033–2053, https://doi.org/10.1007/S11164-016-2745-Y/FIGURES/7.
[88] A.H. Jadhav, K. Lee, S. Koo, J.G. Seo, Esterification of carboxylic acids with alkyl halides using imidazolium based dicationic ionic liquids containing bis-trifluoromethane sulfonimide anions at room temperature, RSC Adv. 5 (2015) 26197–26208, https://doi.org/10.1039/C5RA00802F.
[89] A.H. Jadhav, G.M. Thorat, K. Lee, A.C. Lim, H. Kang, J.G. Seo, Effect of anion type of imidazolium based polymer supported ionic liquids on the solvent free synthesis of cycloaddition of CO_2 into epoxide, Catal. Today 265 (2016) 56–67, https://doi.org/10.1016/J.CATTOD.2015.09.048.

[90] A.J. Varma, S.V. Deshpande, J.F. Kennedy, Metal complexation by chitosan and its derivatives: a review, Carbohydr. Polym. (2004), https://doi.org/10.1016/j.carbpol.2003.08.005.
[91] P. Komadel, J. Madejová, M. Janek, W.P. Gates, R.J. Kirkpatrick, J.W. Stucki, Dissolution of hectorite in inorganic acids, Clays Clay Min. 44 (1996) 228–236, https://doi.org/10.1346/CCMN.1996.0440208.
[92] H. Chen, H. Cheng, F. Zhou, K. Chen, K. Qiao, X. Lu, P. Ouyang, J. Fu, Catalytic fast pyrolysis of rice straw to aromatic compounds over hierarchical HZSM-5 produced by alkali treatment and metal-modification, J. Anal. Appl. Pyrolysis 131 (2018) 76–84, https://doi.org/10.1016/J.JAAP.2018.02.009.
[93] H.W. Lee, Y.M. Kim, B. Lee, S. Kim, J. Jae, S.C. Jung, T.W. Kim, Y.K. Park, Catalytic copyrolysis of torrefied cork oak and high density polyethylene over a mesoporous HY catalyst, Catal. Today 307 (2018) 301–307, https://doi.org/10.1016/J.CATTOD.2017.01.036.
[94] E. Inger, A.K. Sunol, N. Sahiner, Catalytic activity of metal-free amine-modified dextran microgels in hydrogen release through methanolysis of $NaBH_4$, Int. J. Energy Res. 44 (2020) 5990–6001, https://doi.org/10.1002/er.5395.
[95] E. Inger, S. Demirci, M. Can, A.K. Sunol, G. Philippidis, N. Sahiner, PEI modified natural sands of Florida as catalysts for hydrogen production from sodium borohydride dehydrogenation in methanol, Int. J. Energy Res. 45 (2021) 4048–4067, https://doi.org/10.1002/ER.6060.
[96] S. Demirci, A.K. Sunol, N. Sahiner, Catalytic activity of amine functionalized titanium dioxide nanoparticles in methanolysis of sodium borohydride for hydrogen generation, Appl. Catal. B Environ. 261 (2020), 118242, https://doi.org/10.1016/j.apcatb.2019.118242.
[97] G.A. Somorjai, Y. Li. Introduction to Surface Chemistry and Catalysis, 2nd ed., Wiley, 2010, pp. 0–800.